Introduction

The junctional complex, which consists of tight junctions (TJs), adherens junctions (AJs), and desmosomes (DSs), is a hallmark of epithelial cell types in vertebrates [1]. The junctional complex plays crucial roles in mechanical adhesion between epithelial cells to form cellular sheets (AJs and DSs), as well as regulation of paracellular transport to maintain ionic homeostasis between different body compartments (TJs) [2–4,31]. Previous studies have identified a number of molecular constituents for each junction type in the junctional complex, enabling molecular characterization of the structure and function of each junction. One of the common features of these cell–cell junctions is the connection of adhesion molecules in the plasma membrane with cytoskeletons via cytoplasmic plaque proteins [2–4,31]. In addition to these structural proteins, a number of signaling molecules localized at the cytoplasmic region of the junctional complex are thought to be involved in the functional regulation of each cell–cell junction, cell growth, and morphogenesis of epithelial polarity [2–4,31].

An optimal approach to identify molecular constituents of each cell–cell junction is the purification of these structures followed by protein analyses of their components. Among the elements of the junctional complex, the purification of DSs from calf muzzles has been demonstrated, and various DS-associated proteins, including desmogleins and desmoplakins, have been identified from this DS fraction in one-dimensional SDS-PAGE [5,6]. In contrast, the purification of TJs and AJs was less successful [7,8], although alternatively, the production of monoclonal antibodies is a promising technique to identify the molecular constituents of these structures [9,10]. For example, several TJ-associated proteins including ZO-1 and occludin were discovered by the localization-based screening of monoclonal antibodies generated against a TJ-enriched plasma membrane fraction isolated from rodent or avian tissues [9,10]. However, a limitation of this approach is that it depends on the antigenicity, which cannot be controlled. In addition to biochemical and immunological approaches, searches for binding partners of cell–cell junction-associated proteins by co-precipitation and yeast two-hybrid screening have also identified many novel cell–cell junction-related molecules. Nevertheless, there are likely to be yet unidentified proteins localized at the junctional complex. Identification and characterization of these novel molecular components are important for further understanding of the structure and functional regulation of each junction at the molecular level.

To complement these biochemical and immunological approaches, the localization-based expression cloning would be useful to identify cDNAs for novel components of the junctional complex. In this 'visual screening' method, green fluorescent protein (GFP)-fused cDNA or genomic library is initially introduced into the cells. The cells in which exogenous GFP-fusion proteins are localized at certain cellular structures are then selected by fluorescence microscopy, and their cDNAs are cloned. This localization-based screening was first described in *Schizosaccharomyces pombe* [32], and then in mammalian cultured cells to identify a new type of nuclear envelope membrane protein [33]. Furthermore, Kitamura et al. developed the fluorescence localization-based retrovirus-mediated expression cloning (FL-REX) by the use of a retrovirus vector, which allows controllable introduction of cDNA libraries into cells with high-efficiency [11]. However, as of yet, reports on further applications of this method are limited [12].

In this study, we evaluated the FL-REX in obtaining cDNAs of novel molecular constituents localized at TJs and AJs in epithelial cells. We have confirmed that various cDNAs for known TJ- or AJ-associated proteins could be cloned in the FL-REX. Further, using this method we have identified two putative GTPase activating proteins (GAPs) for small G proteins as novel components of the junctional complex. Using in-house generated polyclonal antibodies (pAbs) for these GAPs, they were found to be localized at AJs in various epithelial tissues. These data suggest that FL-REX is a powerful tool to identify novel molecular constituents of the junctional complex.

Materials and methods

Cell culture and transfection

Epithelial cell lines, MDCK II, CSG120/7, and EpH4 were kindly provided by Dr. M. Murata (The University of Tokyo, Tokyo, Japan), Dr. W. Birchmeier (Max-Delbruck-Center for Molecular Medicine, Berlin, Germany), and Dr. E. Reichmann (University Children's Hospital Zurich, Zurich, Switzerland). A potent retrovirus packaging cell line, Plat-E [13], was kindly gifted by Dr. T. Kitamura (The University of Tokyo, Tokyo, Japan). All cells were grown in Dulbecco's modified Eagle's medium supplemented with 10% fetal calf serum. To establish the MDCK II cells competent to mouse retrovirus infection, the ecotropic mouse retrovirus receptor (EcoVR) cDNA (provided by Dr. T. Kitamura) was subcloned into pCAGGS-neodelEcoRI [14] and transfected to MDCK II cells with LipofectAMINE with Plus reagent (Invitrogen, Carlsbad, California, USA). One G418-resistant clone, MDCKIIVR20, was used for the expression cloning.

Construction of the cDNA library for FL-REX

A mouse retrovirus vector, pMX, was kindly provided by Dr. T. Kitamura. To avoid the background fluorescence of native GFP from the vector without cDNA insert in the cDNA–GFP-fusion library, we initially generated pMX-EGFPN-Met(–), a pMX-derived vector containing the EGFP sequence (CLONTCH) in which the ATG codon for the first methionine was deleted, and the EcoRI site with the DNA sequence encoding four glycines were inserted instead. For the construction of the cDNA library, poly(A) + RNA was isolated from CSG120/7 epithelial cells [15] using FastTrack (Invitrogen). The cDNA was synthesized from the poly(A) + RNA with random primers using Time Saver™ cDNA Synthesis Kit (Amersham, Mountain View, California, USA). The cDNA fragments longer than 1kb were size-fractionated from the agarose gel using GFX™ PCR DNA and Gel Band Purification Kit (GE Healthcare, Little Chalfont, Buckinghamshire, England) and were inserted into the EcoRI site of pMX-EGFPN-Met(–), upstream of EGFP cDNA. The ligated DNA was electroporated into DH5a competent cells (Electromax DH5a; Invitrogen) by Gene Pulser (BioRad, Hercules, California, USA). Plasmid DNA was purified after 12h culture

Table 1 – Known TJ- and AJ-associated proteins identified in the FL-REX in this study

Protein	Encoded (total) amino acids	Reported localization
Claudin-2*	1–207 (230)	TJ
Claudin-3*	2–211 (219)	TJ
Claudin-4*	1–189 (210)	TJ
Claudin-7*	1–197 (211)	TJ
CAR*	1–287 (365)	TJ
ZO-1	1–309 (1745)	TJ
ZO-2	1–486 (1167)	TJ
α-catenin	634–875 (906)	AJ
β-catenin	1–719 (781)	AJ
Plakoglobin*	82–472 (745)	AJ
α-actinin-4*	125–624 (912)	AJ
Shroom2	1–348 (1487)	AJ

*Multiple clones were obtained and their representative data presented.

in 200ml of LB medium. The resulting library contained 4.9×10^6 independent clones with an average insert size of 1.3kb. The cDNA library was then converted to the high titer retroviruses in Plat-E packaging cells as described previously [11].

Localization-based expression screening

MDCKIIVR20 cells were infected with the retrovirus library at ~ 20% infection efficiency as described previously [12]. After two days, infected cells were trypsinized, and the GFP-positive cells collected by fluorescence-activating cell sorting (FACS) and sparsely plated on glass-based dishes (IWAKI, Tokyo, Japan). 48–72h after plating the cells were scanned under an Olympus IX71 fluorescence microscope (Olympus, Tokyo, Japan), and cell colonies that contain cells with GFP signals of cell–cell junctions were marked. At the same time the surrounding colonies were scraped with needles under a phase contrast microscope and removed by aspiration. After 4–5 days expansion, the positive colonies were picked up, trypsinized, and replated on the glass-based dishes. Cell clones showing the junctional staining were then selected under a fluorescent microscope, picked up in the same way, and expanded to prepare their genomic DNAs which were used as a template for PCR to recover the integrated cDNA with two primers (GGTGGACCATCCTCTAGACT and GTCGCC-GTCCAGCTCGAC). By the use of cDNA databases, full-length cDNAs were cloned by RT-PCR from total RNA of EpH4 cells. In six experiments ~ 1.2×10^6 cells in total with GFP fluorescence were collected by FACS and subjected to the screening.

Antibodies

Bacterial expression constructs of the GST fusion proteins containing aa. 72–226 of ARHGAP12 and aa. 1040–1412 of SPAL3 were generated by subcloning the corresponding DNA fragments amplified by PCR into pGEX4T-1 (Amersham). Each fusion protein was then produced in *Escherichia coli*, purified with glutathione-Sepharose 4B beads (Amersham), and injected subcutaneously into rabbits to raise polyclonal antibodies (pAbs). The identical antigen regions of ARHGAP12 and SPAL3 were also subcloned into pMAL-c2 (New England Laboratory, Wobum, Massachusetts, USA) to produce maltose-

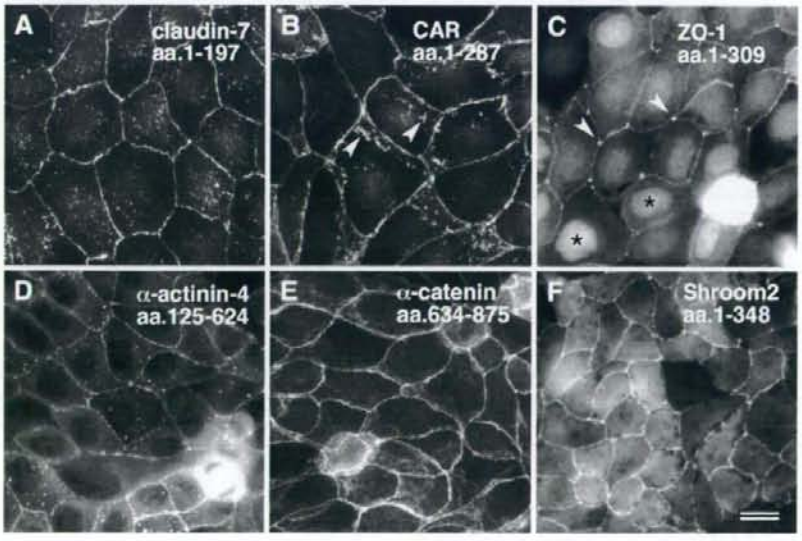

Fig. 1 – Fluorescent images of GFP-fusions localizing at cell–cell junctions in MDCK cells. In the FL-REX using a retrovirus expression library generated from CSG120/7 cells, various GFP-fusions with known TJ- and AJ-associated proteins were obtained. Six examples are shown. (A) claudin-7 (aa. 1–197), (B) CAR (aa. 1–287), (C) ZO-1 (aa. 1–309), (D) α-actinin-4 (aa. 125–624), (E) α-catenin (aa. 634–875), and (F) shroom2 (aa. 1–348). A GFP-fusion with CAR (aa. 1–287) localized at the lateral plasma membrane of MDCK cells as well as at cell–cell junctions as patches (arrowheads in B). A GFP-fusion with ZO-1 (aa. 1–309) was localized at nuclei and tricellular contacts (asterisks and arrowheads in C, respectively) in addition to cell–cell junctions. Scale bars; 10 μm.

binding protein fusions. For affinity purification of the pAbs, bacterial lysates of maltose-binding protein-ARHGAP12 and -SPAL3 fusion proteins were subjected to SDS-PAGE and blotted to nitrocellulose membranes. Membrane pieces blotted with the fusion proteins were incubated with the rabbit sera. After washing with PBS, the bound pAbs were collected by treatment of membranes with 0.2M citrate buffer (pH 2.3). Anti-E-cadherin mAb (ECCD-2) was kindly provided by Dr. M. Takeichi (Riken Center for Developmental Biology, Kobe, Japan). Anti-nectin-2 mAb was kindly provided from Dr. Y. Takai (Osaka University, Osaka, Japan). Anti-occludin mAb MOC37 was generated and characterized as described previously [35]. Anti-ZO-1 mAb R26.4 developed by Dr. D. Goodenough [9] was obtained from the Developmental Studies Hybridoma Bank, developed under the auspices of the NICHD and maintained by The University of Iowa, Department of Biological Sciences, Iowa City, IA 52242.

Immunofluorescence microscopy

Specimens for immunofluorescence microscopy were prepared as described previously [10]. To analyze the distribution of proteins in cultured cells, cells grown on glass coverslips were fixed with 1% formaldehyde in PBS for 15min at room temperature, permeabilized with 0.2% triton X-100 in PBS for 15min, and then washed three times with PBS. After blocking with 1% bovine serum albumin in PBS for 15min, samples were treated with primary antibodies and washed with PBS followed by treatment of secondary antibodies. For immunolocalization of proteins in mouse tissues, frozen sections (~ 5μm thick) of various mouse tissues embedded in O.C.T compound were cut in a cryostat, mounted on glass coverslips, air-dried, and fixed with 95% ethanol at − 20°C for 30min followed by 100% acetone at room temperature for 1min. After being washed with PBS, sections were blocked with 1% bovine serum albumin for 15min, treated with primary antibodies, and washed with PBS followed by treatment with secondary antibodies. After being washed with PBS, samples were mounted in 30% MOWIOL (CALBIOCHEM, La Jolla, California, USA). Specimens were observed using an Olympus IX70 fluorescence microscope (Olympus), a Zeiss Axio-phot photomicroscope, or Zeiss LSM510 confocal laser-scanning microscope (Carl Zeiss, Jena, Germany).

Results

Cloning of known cDNAs for TJ- and AJ-associated proteins in the FL-REX

In the present study, to improve the efficiency of the FL-REX for the screening and identification of novel components localized at the epithelial junctional complex, we adopted several modifications to reported methods. First, we created a cDNA–GFP-fusion library from the transcripts of CSG120/7 epithelial cells, a cell line derived from the mouse salivary gland. Secondly, to construct the retrovirus expression library for cDNA–GFP-fusions, the ATG codon of the first methionine of GFP in the vector was deleted in advance to avoid the background signal of native GFP from vectors without cDNAs, which are located upstream of GFP. This appeared to be effective as the ratio of cells with GFP signals in total cells infected with the retrovirus cDNA–GFP library was ~ 0.4% in this study, compared with 4% in the study by Nishimura et al., who preserved the initiation ATG of GFP [12]; infection efficiency approximately 20% in both studies. Next, cells were grown on glass-based culture plates instead of plastic ones to increase the detection sensitivity of GFP signal under the visual screening with an inverted fluorescence microscope.

Since TJs and AJs circumscribe the cells at the most apical part of the lateral plasma membrane, cells showing concentration of GFP-fusions into the apical cell–cell junction could be easily identified in the FL-REX. From ~ 1.2×10^6 GFP-positive cells collected by FACS in six experiments, we obtained a number of GFP-fusions with known TJ- and AJ-associated proteins (Table 1). The typical localization of these GFP-fusions

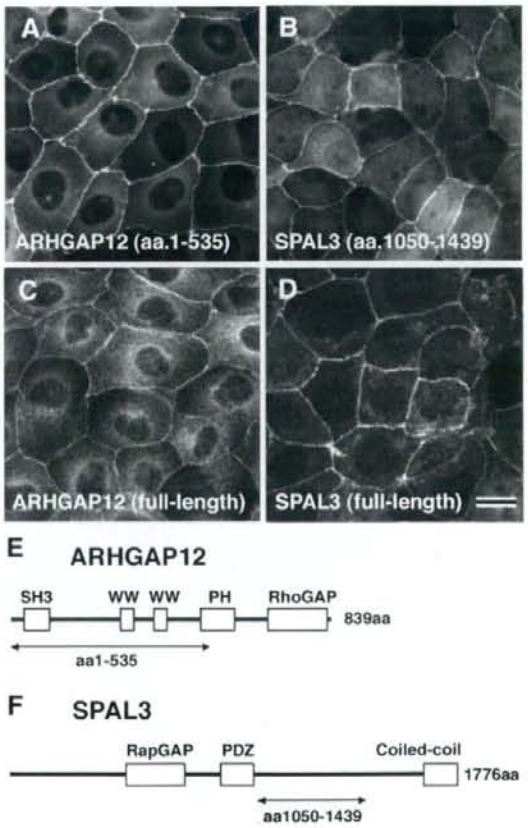

Fig. 2 – Identification of ARHGAP12 and SPAL3 as novel components of epithelial cell–cell junctions by the FL-REX. GFP-fusions with ARHGAP12 aa. 1–535 (A) and with SPAL3 aa. 1050–1439 (B) were concentrated at cell–cell junctions of MDCK cells in the FL-REX. Full-length ARHGAP12 (C) and SPAL3 (D) fused with GFP were also localized at cell–cell junctions. Domain structures of ARHGAP12 and SPAL3 were predicted by Pfam and SMART programs, and shown in (E) and (F) respectively. Scale bars; 10 μm.

in MDCK cells are shown in Fig. 1. The most abundant TJ proteins found by our screening were claudins, including claudin-2, -3, -4, and -7. cDNAs of claudins were obtained in every ~ 10^4 GFP-positive cells; this frequency was much higher than that of other junctional molecules (data not shown). cDNAs for other TJ-associated proteins CAR, ZO-1, and ZO-2 were also cloned in this screening. As cDNAs of known AJ-associated proteins, partial sequences of α-catenin, β-catenin, plakoglobin, α-actinin-4, and shroom2 were obtained.

Among these GFP-fusions, non-cell–cell junctional localizations were also observed. For example, CAR (aa. 1–287)–GFP-fusion was often detected as patches at the basolateral membrane of MDCK cells (Fig. 1B). In addition, ZO-1 (aa. 1–309)–GFP-fusion was localized at the nucleus and cytoplasm, and its concentration at tricellular contacts was remarkable (Fig. 1C). These localizations are likely to be artifacts as both proteins are known to be highly concentrated at tight junctions [7,34]. In contrast, strengthened localization of GFP-fusions into cell–cell junctions was also observed. α-catenin (aa. 634–875) showed a high concentration at the apical cell–cell junction (Fig. 1E), although endogenous α-catenin is distributed throughout the lateral plasma membrane including the apical cell–cell junction (data not shown).

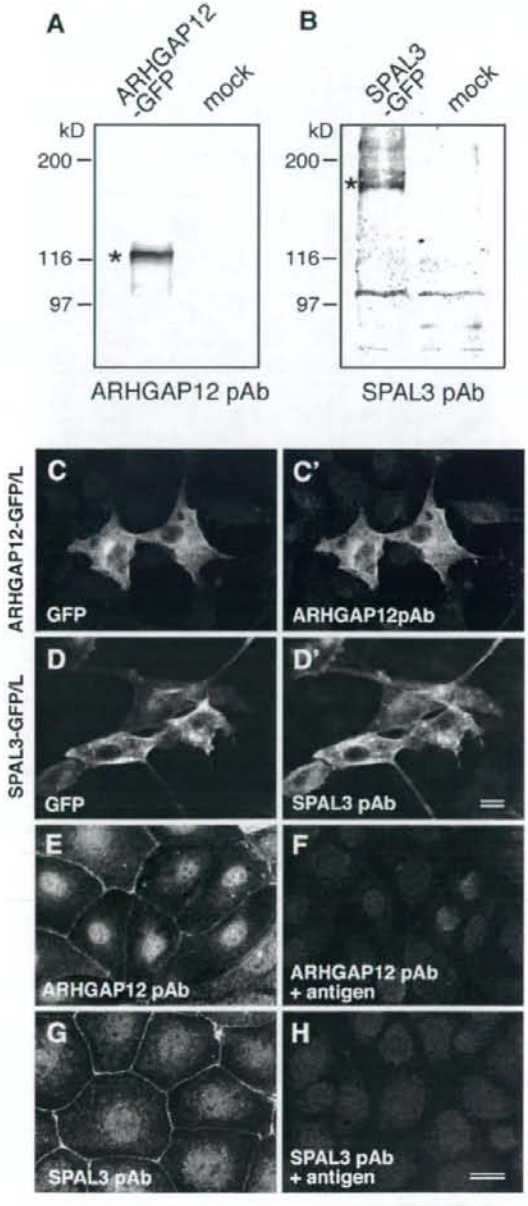

Identification of ARHGAP12 and SPAL3, putative GTPase activating proteins for small G proteins, as components of epithelial cell–cell junctions

In the FL-REX screening based on the junctional localization, we have cloned GFP-fusions containing partial cDNAs for two putative GTPase activating proteins (GAPs) for small G proteins, neither of which have been reported to be localized at epithelial cell–cell junctions. One GFP-fusion contained aa. 1–535 of ARHGAP12 (GenBank accession no. NM029277), a putative Rho GTPase activating protein, whose cloning in human has been reported already (Fig. 2A) [16]. ARHGAP12 contains Src homology 3 (SH3) domain, two conserved tryptophans (WW) domain, pleckstrin homology (PH) domain, and Rho GAP domains in this order (Fig. 2E), and this overall domain structure is shared by other potential Rho GAPs including ARHGAP9 and ARHGAP15 [17]. Another GFP-fusion contained aa. 1050–1439 of SPAL3 (GenBank accession no. NM001081028) (Fig. 2C), a putative Rap GTPase activating protein. SPAL3 is closely related to SPAL (SPA-1 like-protein),

Fig. 3 – Evaluation of the specificity of anti-ARHGAP12 pAb and anti-SPAL3 pAb. (A), (B) Western blotting. Cell lysates of HEK293 cells expressing GFP-tagged full-length ARHGAP12 (ARHGAP12-GFP) or GFP-tagged SPAL3 aa. 341–1776 (SPAL3-GFP) were immunoblotted with anti-ARHGAP12 pAb (A) or anti-SPAL3 pAb (B). Asterisks indicate specific bands of ARHGAP12-GFP and SPAL3 aa. 341-1776-GFP respectively. Both antibodies did not recognize endogenous proteins in the lysate of parent HEK293 loaded on the same membranes (mock). (C–D') Immunostaining. ARHGAP12-GFP-expressing L cells (ARHGAP12-GFP/L) (C and C') and SPAL3-GFP-expressing L cells (SPAL3-GFP/L) (D and D') grown on coverslips were immunostained with anti-ARHGAP12 pAb (C') and anti-SPAL3 pAb (D'). The GFP signals from ARHGAP12-GFP (C) and SPAL3-GFP (D) completely overlapped with intensive signals of antibody staining. (E) Immunofluorescent image of EpH4 cells stained with anti-ARHGAP12 pAb. The junctional staining was undetectable after pretreatment of the primary antibody solution with an excess amount of the recombinant MBP-ARHGAP12 (aa. 72–226) protein (F). (G) The immunofluorescence image of EpH4 cells stained with anti-SPAL3 pAb. The junctional staining was undetectable after pretreatment of the primary antibody solution with an excess amount of the recombinant MBP-SPAL3 (aa. 1040–1412) fusion proteins (H). Scale bars; 10 μm.

which was originally identified as a binding protein of PSD-95/SAP90, a scaffold protein of the post-synaptic density [18]. Similar to SPAL, SPAL3 contains Rap GAP, PDZ, and coiled–coil domains in this order (Fig. 2F). We then cloned full-length cDNAs of ARHGAP12 and SPAL3 in mice, and confirmed that their full-length constructs with GFP-tags were recruited to cell–cell contact sites when overexpressed in MDCK cells (Fig. 2B, D).

Since GFP-fusion with aa. 1–535 of ARHGAP12 containing SH3 domain and two WW domains localize at cell–cell junctions, we attempted to identify which domain is required for this localization. We constructed ARHGAP12-GFP mutants in which the SH3 domain (aa. 13–71) or two WW domains (aa. 263–388) were deleted, and produced MDCK cells stably expressing these deletion mutants. In fluorescence microscopy, however, neither of these constructs concentrated into cell–cell junctions (Fig. S1).

Generation of antibodies for ARHGAP12 and SPAL3

To examine the tissue expression and the subcellular localization of ARHGAP12 and SPAL3, we raised rabbit polyclonal antibodies for these proteins. In Western blotting of the membrane on which cell lysates of GFP-tagged ARHGAP12-overexpressing HEK293 cells were loaded, anti-ARHGAP12 antibody recognized a band of ~ 120kDa, which is consistent with the mass of molecular weights of GFP (27kDa) and ARHGAP12 (92kDa) (Fig. 3A). Similarly, in the lysates of HEK293 cells overexpressing GFP-tagged SPAL3 aa. 341–1776, anti-SPAL3 antibody recognized a band of ~ 180kDa, which is consistent with the mass of the putative molecular weights of GFP (27kDa) and SPAL3 aa. 341–1776 (158kDa) (Fig. 3B). Both antibodies could not detect endogenous proteins in the lysate of parent HEK293. To evaluate the ability of these antibodies for immunostaining, mouse L fibroblasts transiently transfected with expression vectors for GFP-tagged mouse ARHGAP12 or GFP-tagged SPAL3 were labeled with these antibodies. As shown in Fig. 3C–D', anti-ARHGAP12 antibody and anti-SPAL3 antibody intensively recognized only cells with GFP signals from GFP-ARHGAP12 and GFP-SPAL3 respectively. Moreover, when EpH4 cells were immunolabeled with these antibodies, the staining patterns of cell–cell junctions were observed around the cells (Fig. 3E, G). No staining was observed following pretreatment of primary antibodies with excess recombinant antigens, indicating that endogenous ARHGAP12 and SPAL3 are localized at cell–cell junctions in EpH4 epithelial cells (Fig. 3F, H). Neither anti-ARHGAP12 nor anti-SPAL3 antibodies we generated could detect endogenous ARHGAP12 or SPAL3 protein in EpH4 cells in Western blotting probably because of their weak reactivities to blotted proteins. However, the transcripts of both proteins were detected by RT-PCR in various mouse cultured cell lines including epithelial cells, fibroblasts, and teratocarcinoma cells such as EpH4, CSG120/7, L, NIH3T3, and F9 cells (data not shown).

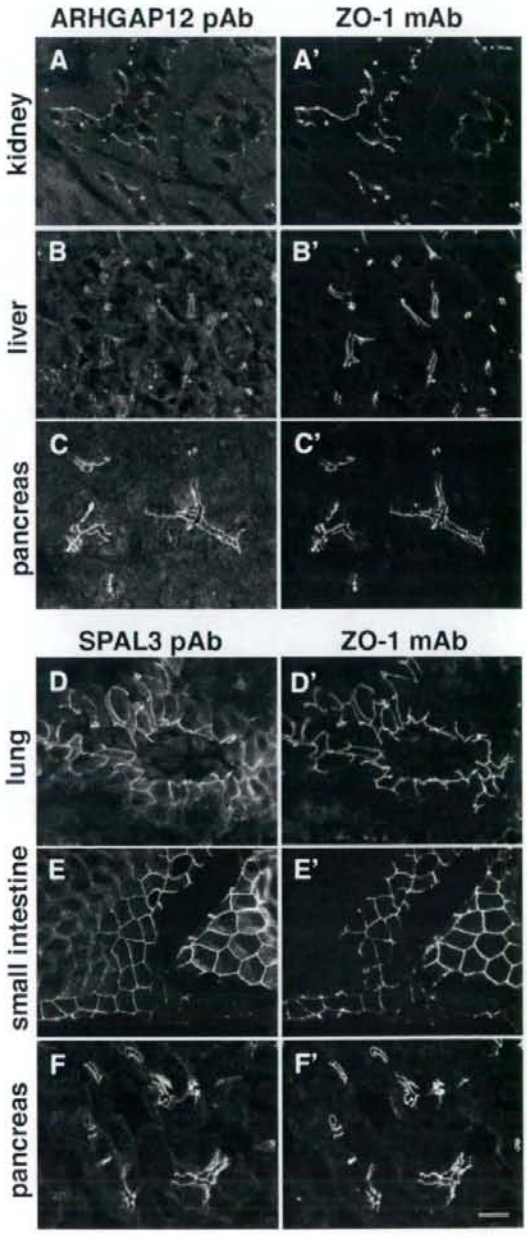

Fig. 4 – Immunolocalization of ARHGAP12 and SPAL3 in mouse tissues. Upper panel: frozen sections of mouse kidney, liver, and pancreas were double stained with anti-ARHGAP12 pAb (A–C) and anti-ZO-1 mAb (A'–C'). Fluorescent signals from ARHGAP12 and ZO-1 were mostly overlapped at cell–cell junctions of renal epithelial cells in the kidney (A and A'), hepatocytes in the liver (B and B'), and exocrine cells in the pancreas (C and C'). Lower panel: frozen sections of mouse lung, small intestine, and pancreas were double stained with anti-SPAL3 pAb (D–F) and anti-ZO-1 mAb (D'–F'). Fluorescent signals from SPAL3 and ZO-1 were mostly overlapped at cell–cell junctions of bronchial epithelial cells in the lung (D and D'), intestinal epithelial cells (E and E'), and exocrine cells in the pancreas (F and F'). Scale bars; 10 μm.

Subcellular localization of ARHGAP12 and SPAL3

Localization of ARHGAP12 and SPAL3 in mouse tissues was analyzed by immunofluorescence microscopy. Tissue sections were double-stained with either pAb of these GAPs and a mAb of ZO-1. ZO-1 is localized at TJs in epithelial cells, but is often used as a good marker for the junctional complex including TJs and AJs at the conventional fluorescence microscopy since its concentration into cell–cell contacts is remarkably clear compared with those of AJ-components such as E-cadherin and nectins, which are also localized at the basolateral membrane domain. As shown in Fig. 4, ARHGAP12 was localized at the junctional complex of tissues including the small intestine, the kidney, the salivary gland, and the liver. SPAL3 was detected at the junctional complex of various tissues including the lung, the small intestine, the kidney, and the salivary gland. In addition to the junctional complex, staining signals of ARHGAP12 and SPAL3 were detected in the cytoplasm and the basolateral membrane respectively, each of which appeared to be specific; pretreatment of the antibody with excess recombinant antigen of each protein abolished staining (data not shown). We observed no detectable ARHGAP12 or SPAL3 staining in blood vessels, suggesting that both GAPs are localized at cell–cell junctions in epithelial cells, but not in endothelial cells (data not shown).

To determine the precise localization of ARHGAP12 and SPAL3 within the junctional complex, double immunofluorescence staining of mouse small intestine was performed, and expression of these GAPs were compared with that of occludin [10], a marker for TJs, and E-cadherin and nectin-2 [19], markers for AJs, by confocal laser-scanning microscopy. As shown in Fig. 5, junctional expression of ARHGAP12 was more basal than that of occludin, and mostly overlapped with E-cadherin and nectin-2. SPAL3 showed the same distribution (Fig. 5). These results indicate that ARHGAP12 and SPAL3 are localized at AJs in the junctional complex of epithelial cells.

Localization of these GAPs at AJs suggested the possibility that these proteins are recruited to AJs by interacting with components of cadherin-mediated cell–cell adhesion. Thus, we examined the localization of these proteins in EL cells in immunofluorescence microscopy. EL cells were established from mouse L cells, which lack cadherin-mediated adhesion, by the stable introduction of E-cadherin [38]. EL cells exhibit E-cadherin-dependent cell–cell adhesion, and it has been reported that basic components of cadherin-mediated cell–cell adhesion such as E-cadherin, α-catenin, β-catenin are concentrated into cell–cell contact sites of EL cells [39]. In immunofluorescence staining, interestingly, endogenous SPAL3 was clearly colocalized with E-cadherin at cell–cell contact sites in EL cells whereas it was distributed in the cytoplasm in L cells (Fig. 6), suggesting the interaction of SPAL3 with basic components of cadherin-mediated cell–cell adhesion. The staining signal of EL cells with anti-ARHGAP12 pAb was very faint and its concentration at cell–cell contact sites was not detected (data not shown). Although this might be due to the low expression level of ARHGAP12 in EL cells, exogenous ARHGAP12-GFP expressed by transient transfection was not concentrated at cell–cell contact sites, or neither (data not shown).

Discussion

There is only one prior report of FL-REX used for the cDNA cloning of cell–cell junction-associated proteins [12]. In that study fluorescence-activating cell sorting (FACS) was introduced into the original FL-REX method, and the tight junction-associated protein identified JEAP was identified using a cDNA library generated from an endothelial cell line. However, further application of this method has not been reported. In this study, we adopted several modifications to previous methods to improve the efficiency of the screening, and suggest that the FL-REX is a useful tool to identify novel components of TJs and AJs as a complement to biochemical and immunological approaches.

The FL-REX has several advantages compared to biochemical approaches in the identification of novel proteins localizing at intercellular junctions, and also at various cellular structures. First, novel proteins can be obtained without purification of the cellular structure, which is often very difficult. Thus, the FL-REX is useful as far as cDNA libraries are available. Usually, only limited sources can be used for biochemical purifications of certain cellular structures. In contrast, the FL-REX is applicable to various cDNA sources, including most tissues and cell lines, as the established method for the cDNA library production is common to all sources. Secondly, since screening is performed in the native condition in living cells, proteins can be identified that are typically lost during biochemical isolation of cellular structures due to their low affinity with them. Previously reported isolation methods for intercellular junctions often expose the junctional membranes to unphysiological conditions, such as hypotonic buffer solution [7,8], in which some protein–protein interactions might be disrupted. These problems can be excluded in the FL-REX.

Conversely, there are also some problems in FL-REX. When expression cloning is performed with conventional cDNA libraries prepared from cellular poly(A)+RNAs, the efficiency of the cloning for given cDNAs is dependent on their expression levels, implying that cloning of cDNAs with low expression is difficult. Furthermore, localization domains should have correct conformations in GFP-fusions to show the correct subcellular localization. These limitations may account for our results demonstrating that claudins were cloned in our screening in much higher frequency than other junctional proteins. The construction of averaged cDNA libraries might overcome these problems to clone a different set of cDNAs. We have already confirmed that the use of cDNA libraries generated from cDNAs with different average sizes, or from different sources, provides different spectra of obtained cDNAs for AJ- and TJ- associated proteins (unpublished data), and further screening is ongoing in our laboratory.

In the present study, using the FL-REX method we cloned two putative GAPs for small G proteins, ARHGAP12 and SPAL3, as novel components of AJs. AJs circumscribe epithelial cells at their apical margins with actin filaments closely apposed to the membranes on the cytoplasmic side [1,2]. One of the important regulators of the actin cytoskeleton is the Rho family GTPase, which includes Rho, Rac, and Cdc42. Accumulating evidence suggests that this family are also involved in

the formation and function of AJs and TJs, probably through rearrangement of actin filaments [20,21]. The activities of Rho family GTPases are spatially and temporally controlled by guanine nucleotide exchange factor (GEF), which exchanges GDP for GTP, and GTPase activating protein (GAP), which accelerates the GTPase activity. To date, several GEFs and

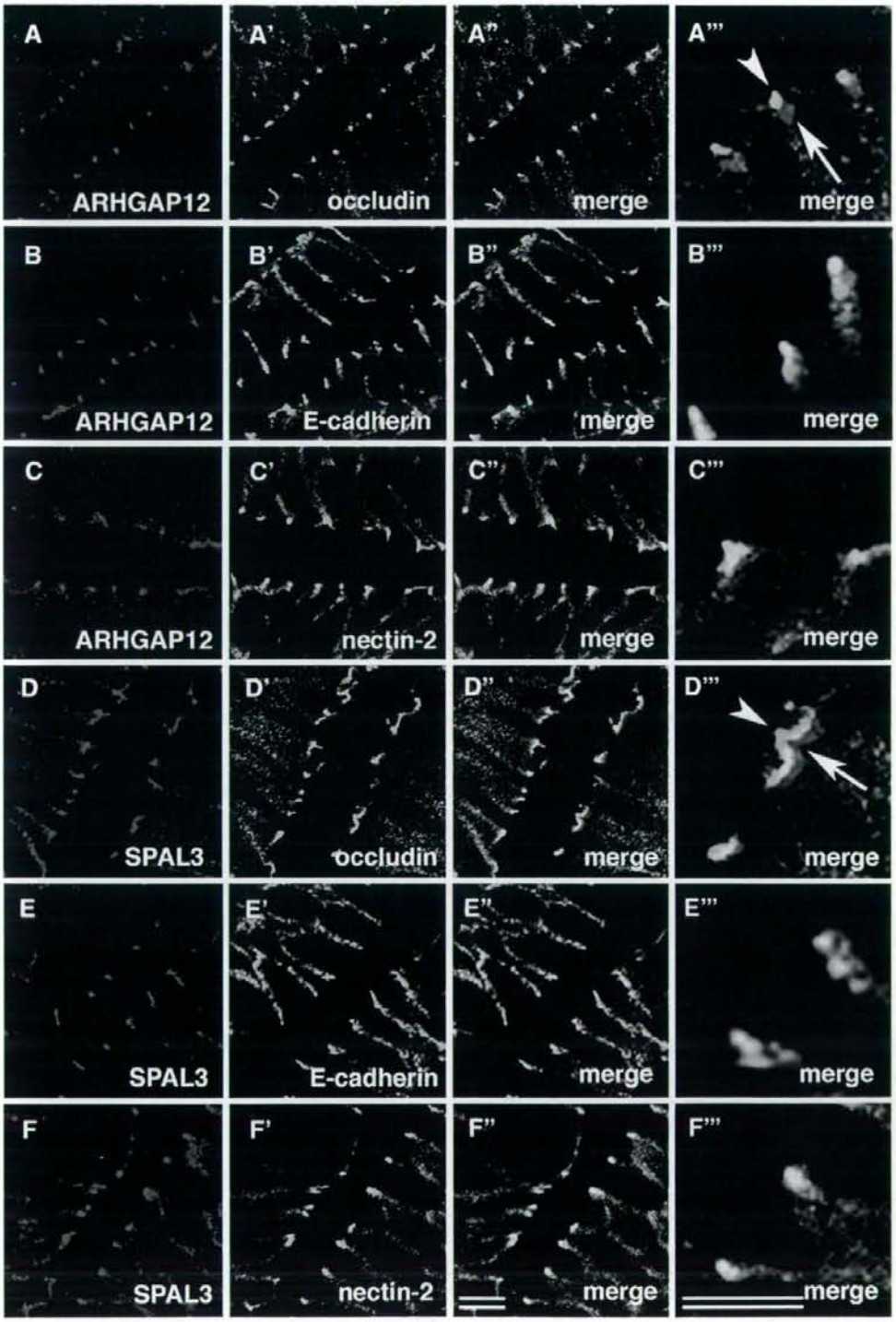

GAPs of Rho family GTPases have been demonstrated to be involved in the formation and configuration of TJs and AJs in epithelial cells [22–24].

ARHGAP12 is a member of closely related Rho GAPs including ARHGAP9 and ARHGAP15 [17]. ARHGAP9 demonstrated substantial GAP activity toward Cdc42Hs and Rac1, and its overexpression in human leukemia cells resulted in the repression of adhesion of cells to the extracellular matrix [25]. ARHGAP15 showed Rac1-specific GAP activity, and its overexpression in HeLa cells resulted in an increase in actin stress fibers and cell contraction [17]. Since ARHGAP12 is closely related to ARHGAP9 and 15, one possibility is that ARHGAP12 is involved in the regulation of AJ formation by spatially suppressing the activity of Rac1 and/or Cdc42 at AJs, although the specificity of GAPs has to be determined *in vivo* in each specific cell type. Alternatively ARHGAP12 may be involved in some other functions triggered by junction assembly. Since ARHGAP12 mutants, which lack either SH3 domain or WW domain, did not concentrate into cell–cell contacts in epithelial cells, both domains seems to be required for the localization of ARHGAP12 at AJs. It has been reported that SH3 domains of vinexin bind to vinculin [36] and lp-dlg [37], both of which are localized at AJs. Therefore, the SH3 domain of ARHGAP12 may also interact with these proteins. To date, the interaction of the WW domain with AJ-associated proteins has not been reported.

The sequence similarity of SPAL3 with those of SPA-1 and SPAL [18,26], both of which are Rap-GAPs, suggests that SPAL3 is also a Rap-specific GAP. Although Rap1 has been implicated in the control of integrin-mediated cell adhesion, recent evidence indicates that Rap1 also plays an important role in cadherin-mediated cell adhesion, including adherens junction formation [27]. Rap1 activity rescued Ras-induced disruption of cell–cell adhesion in MDCK cells and hepatocyte growth factor-induced cell scattering, suggesting that Rap1 positively regulates cadherin-based cell–cell adhesion [28]. Further, Hogan et al. reported that C3G, a Rap1GEF, interacts with the cytoplasmic domain of E-cadherin, and that ligation of the extracellular domain of E-cadherin enhances Rap1 activity, which in turn is necessary for the proper targeting of E-cadherin molecules to maturing cell–cell contacts [29]. Takai et al. have recently shown that Rap1 is also involved in adherens junction formation through the nectin–afadin system, another adhesion system of adherens junctions [30]. These observations suggest that SPAL3 may function in adherens junction formation by balancing the role of Rap1 by counteracting RapGEFs. The aa. 1050–1439 of SPAL3, which was required for localization at cell–cell contact sites in epithelial cells, does not contain any known domain structure (Fig. 2B, F). However, the fact that SPAL3 colocalized with E-cadherin at cell–cell contact sites in EL cells suggests that this region of SPAL3 interacts with the basic components of cadherin-mediated cell–cell adhesion, such as E-cadherin, α-catenin, β-catenin, and their binding proteins.

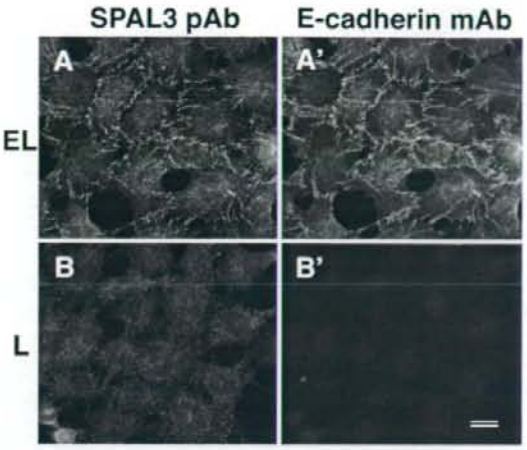

Fig. 6 – Localization of SPAL3 in L cells expressing E-cadherin. Double immunofluorescence staining of EL cells and L cells with anti-SPAL3 pAb (A, B) and anti-E cadherin mAb (A', B'). In EL cells, SPAL3 and E-cadherin were colocalized at cell–cell contact sites (A, A') whereas SPAL3 was distributed in the cytoplasm in L cells (B). Scale bars; 10 μm.

Although, so far, simple overexpression of ARHGAP12 and SPAL3 in EpH4 mouse epithelial cells seems not to affect cell morphology at the confluent condition (data not shown), these GAPs may be involved in the maturation of newly formed cell–cell contacts, the organization of actin stress fibers, or cell adhesion activity. Not only analyses along this line but also studies by knock down, overexpression of their dominant negative forms, and identification of binding partners will lead to better understanding their functions in epithelial AJs.

Acknowledgments

We would like to thank Dr. T. Kitamura for providing all reagents for the FL-REX, Dr. M. Takeichi for anti-E-cadherin mAb and EL

Fig. 5 – Distribution of ARHGAP12 and SPAL3 within the junctional complex. Upper panel: double immunofluorescence staining of mouse small intestine with anti-ARHGAP12 pAb and anti-occludin mAb (A–A'''), with anti-ARHGAP12 pAb and anti-E-cadherin mAb (B–B'''), or with anti-ARHGAP12 pAb and anti-nectin-2 mAb (C–C'''). In the merged image, ARHGAP12 (an arrow) was distributed more on the basal side of intestinal epithelial cells than occludin (an arrowhead) (A'' and A'''), whereas mostly colocalized with E-cadherin (B'' and B''') and nectin-2 (C'' and C''') at the junctional complex. Lower panel: double immunofluorescence staining of mouse small intestine with anti-SPAL3 pAb and anti-occludin mAb (D–D'''), with anti-SPAL3 pAb and anti-E-cadherin mAb (E–E'''), or with anti-SPAL3 pAb and anti-nectin-2 mAb (F–F'''). In the merged image, SPAL3 (an arrow) was distributed more on the basal side of intestinal epithelial cells than occludin (an arrowhead) (D'' and D'''), whereas colocalized with E-cadherin (E'' and E''') and nectin-2 (F'' and F'''). Occludin was used as a marker of TJs, wheareas E-cadherin and nectin-2 were used as markers of AJs. Scale bars; 10 μm.

cells, Dr. Y. Takai for anti-nectin-2 mAb, and Dr. T. Imai (KAN Research Institute, Ltd) and Ms. K. Umeda (Kumamoto University) for technical advice. We also thank Ms. C. Fujiwara for her excellent technical assistance, and all the members of Tsukita and Furuse laboratories for their helpful discussions.

This study was supported by a Grand-in-Aid for Scientific Research (B) from the Japan Society for the Promotion of Science and grants from Takeda Science Foundation and the Uehara Memorial Foundation to M.F.

Appendix A. Supplementary data

Supplementary data associated with this article can be found, in the online version, at doi:10.1016/j.yexcr.2007.11.009.

REFERENCES

[1] M.G. Farquhar, G.E. Palade, Junctional complexes in various epithelia, J. Cell Biol. 17 (1963) 375–412.
[2] A. Nagafuchi, Molecular architecture of adherens junctions, Curr. Opin. Cell Biol. 13 (2001) 600–603.
[3] D.R. Garrod, A.J. Merritt, Z. Nie, Desmosomal adhesion: structural basis, molecular mechanism and regulation, Mol. Membr. Biol. 19 (2002) 81–94.
[4] S. Tsukita, M. Furuse, M. Itoh, Multifunctional strands in tight junctions, Nat. Rev. Mol. Cell. Biol. 2 (2001) 285–2933.
[5] P. Drochmans, C. Freudenstein, J.C. Wanson, L. Laurent, T.W. Keenan, J. Stadler, R. Leloup, W.W. Franke, Structure and biochemical composition of desmosomes and tonofilaments isolated from calf muzzle epidermis, J. Cell Biol. 79 (1978) 427–443.
[6] G. Gorbslky, M.S. Steinberg, Isolation of the intercellular glycoprotein of desmosomes, J. Cell Biol. 90 (1981) 243–248.
[7] B.R. Stevenson, D.A. Goodenough, Zonulae occludentes in junctional complex-enriched fractions from mouse liver: preliminary morphological and biochemical characterization, J. Cell Biol. 98 (1984) 1209–1221.
[8] S.A. Tsukita, S.H. Tsukita, Isolation of cell–cell adherens junctions from rat liver, J. Cell Biol. 108 (1989) 31–41.
[9] B.R. Stevenson, J.D. Siliciano, M.S. Mooseker, D.A. Goodenough, Identification of ZO-1: a high molecular weight polypeptide associated with the tight junction (zonula occludens) in a variety of epithelia, J. Cell Biol. 03 (1986) 755–766.
[10] M. Furuse, T. Hirase, M. Itoh, A. Nagafuchi, S. Yonemura, S.A. Tsukita, S.H. Tsukita, Occludin: a novel integral membrane protein localizing at tight junctions, J. Cell Biol. 123 (1993) 1777–1788.
[11] K. Misawa, T. Nosaka, S. Morita, A. Kaneko, T. Nakahata, S. Asano, T. Kitamura, A method to identify cDNAs based on localization of green fluorescent protein fusion products, PNAS 97 (2000) 3062–3066.
[12] M. Nishimura, M. Kakizaki, Y. Ono, K. Morimoto, M. Takeuchi, Y. Inoue, T. Imai, Y. Takai, JEAP, a novel component of tight junctions in exocrine cells, J. Biol. Chem. 277 (2002) 5583–5587.
[13] S. Morita, T. Kojima, R. Kitamura, Plat-E: an efficient and stable system for transient packaging of retroviruses, Gene Ther. 7 (2000) 1063–1066.
[14] H. Niwa, K. Yamamura, J. Miyazaki, Efficient selection for high-expression transfectants with a novel eukaryotic vector, Gene 108 (1991) 193–200.
[15] M.A. Knowles, L.M. Franks, Stages in neoplastic transformation of adult epithelial cells by 7, 12-dimethylbenz(a)anthracene in vitro, Cancer Res. 37 (1977) 3917–3924.
[16] Z. Zhang, C. Wu, S. Wang, W. Huang, Z. Zhou, K. Ying, Y. Xie, Y. Mao, Cloning and characterization of ARHGAP12, a novel human rhoGAP gene, Int. J. Biochem. 34 (2002) 325–331.
[17] M.L. Seoh, C.H. Ng, J. Yong, L. Lim, T. Leung, ArhGAP15, a novel human RacGAP protein with GTPase binding property, FEBS Lett. 539 (2003) 131–137.
[18] B.C. Roy, K. Kohu, K. Matsuura, H. Yanai, T. Akiyama, SPAL, a Rap-specific GTPase activating protein, is present in the NMDA receptor-PSD-95 complex in the hippocampus, Genes Cells 7 (2002) 607–617.
[19] K. Takahashi, H. Nakanishi, M. Miyahara, K. Mandai, K. Satoh, A. Satoh, H. Nishioka, J. Aoki, A. Nomoto, A. Mizoguchi, Y. Takai, Nectin/PRR: an immunoglobulin-like cell adhesion molecule recruited to cadherin-based adherens junctions through interaction with afadin, aPDZ domain-containing protein, J. Cell Biol. 145 (1999) 539–549.
[20] K. Takaishi, T. Sasaki, H. Kotani, H. Nishioka, Y. Takai, Regulation of cell–cell adhesion by Rac and Rho small G proteins in MDCK cells, J. Cell Biol. 139 (1997) 1047–1059.
[21] T. Jou, E.E. Schneeberger, W.J. Nelson, Structural and functional regulation of tight junctions by RhoA and Rac1 small GTPases, J. Cell Biol. 142 (1998) 101–115.
[22] A.E. Mertens, T.P. Rygiel, C. Olivo, R. van der Kammen, J.G. Collard, The Rac activator Tiam1 controls tight junction biogenesis in keratinocytes through binding to and activation of the Par polarity complex, J. Cell Biol. 170 (2005) 1029–1037.
[23] T. Otani, T. Ichii, S. Aono, M. Takeichi, Cdc42 GEF Tuba regulates the junctional configuration of simple epithelial cells, J. Cell Biol. 175 (2006) 135–146.
[24] C.D. Wells, J.P. Fawcett, A. Traweger, Y. Yamanaka, M. Goudreault, K. Elder, S. Kulkarni, G. Gish, C. Virag, C. Lim, K. Colwill, A. Starostine, P. Metalnikov, T. Pawson, A Rich1/Amot complex regulates the Cdc42 GTPase and apical-polarity proteins in epithelial cells, Cell 125 (2006) 535–548.
[25] Y. Furukawa, T. Kawase, Y. Daigo, T. Nishiwaki, H. Ishiguro, M. Takahashi, J. Kitayama, Y. Nakamura, Isolation of a novel human gene ARHGAP9, encoding a Rho-GTPase activating protein, Biochem. Biophys. Res. Commun. 284 (2001) 643–649.
[26] N. Tsukamokto, M. Hattori, H. Yang, J.L. Bos, N. Minato, Rap1 GTPase-activating proteins SPA-1 negatively regulates cell adhesion, J. Biol. Chem. 274 (1999) 18463–18469.
[27] M.R.H. Kooistra, N. Dube, J.L. Bos, Rap1: a key regulator in cell–cell junction formation, J. Cell Sci. 120 (2007) 17–22.
[28] L.S. Price, A. Hajdo-Milasinovic, J. Zhao, F.J.T. Zwarkruis, J.G. Collard, J.L. Bos, Rap1 regulates E-cadherin-mediated cell–cell adhesion, J. Biol. Chem. 279 (2004) 35127–35132.
[29] C. Hogan, N. Serpente, P. Cogram, C.R. Hosking, C.U. Bialucha, S.M. Feller, V.M. Braga, W. Birchmeier, Y. Fujita, Rap1 regulates the formation E-cadherin-based cell–cell contacts, Mol. Cell Biol. 24 (2004) 6690–6700.
[30] T. Fukuyama, H. Ogita, T. Kawakatsu, T. Fukuhara, T. Yamada, T. Sato, K. Shimizu, T. Nakamura, M. Matsuda, Y. Takai, J. Biol. Chem. 280 (2005) 815–825.
[31] S. Aijaz, M.S. Balda, K. Matter, Tight junctions: molecular architecture and function, Int. Rev. Cytol. 248 (2006) 261–298.
[32] K.E. Sawin, P. Nurse, Identification of fission yeast nuclear markers using random polypeptide fusions with green fluorescent protein, Proc. Natl. Acad. Sci. U. S. A. 94 (1996) 15146–15151.
[33] M.M. Rolls, P.A. Stein, S.S. Taylor, E. Ha, F. McKeon, T.A. Rapoport, A visual screening of a GFP-fusion library identifies a new type of nuclear envelope membrane protein, J. Cell Biol. 146 (1999) 29–44.
[34] E. Raschperger, J. Thyberg, S. Pettersson, L. Philipson, J. Fuxe, R.F. Pettersson, The coxackie- and adenovirus receptor (CAR) is an in vivo marker for epithelial tight junctions, with a potential role in regulating permeability and tissue homeostasis, Exp. Cell Res. 312 (2006) 1566–1580.

[35] M. Saitou, Y. Ando-Akatsuka, M. Itoh, M. Furuse, J. Inazawa, K. Fujimoto, S. Tsukita, Mammalian occludin in epithelial cells: its expression and subcellular distribution, Eur. J. Cell Biol. 73 (1997) 222–231.
[36] N. Kioka, S. Sakata, T. Kawauchi, T. Amachi, S.K. Akiyama, K. Okazaki, C. Yaen, K.M. Yamada, S. Aota, Vinexin: a novel vinculin-binding protein with multiple SH3 domains enhances actin cytoskeletal organization, J. Cell Biol. 144 (1999) 59–69.
[37] M. Wakabayashi, T. Ito, M. Mitsushima, S. Aizawa, K. Ueda, T. Amachi, N. Kioka, Interaction of Ip-dlg/KIAA0583, a membrane-associated guanylate kinase family protein, with vinexin and b-catenin at sites of cell–cell contact, J. Biol. Chem. 278 (2003) 21709–21714.
[38] A. Nagafuchi, Y. Shirayoshi, K. Okazaki, K. Yasuda, M. Takeichi, Transformation of cell adhesion properties by exogenously introduced E-cadherin cDNA, Nature 329 (1987) 341–343.
[39] A. Nagafuchi, M. Takeichi, S. Tsukita, The 102 kd cadherin-associated protein: similarity to vinculin and posttranscriptional regulation of expression, Cell 65 (1991) 849–857.

J Appl Physiol 104: 766–772, 2008.
First published January 10, 2008; doi:10.1152/japplphysiol.00870.2007.

Cyclic strain induces mouse embryonic stem cell differentiation into vascular smooth muscle cells by activating PDGF receptor β

Nobutaka Shimizu,[1,2]* Kimiko Yamamoto,[1,3]* Syotaro Obi,[1] Shinichiro Kumagaya,[1] Tomomi Masumura,[1] Yasumasa Shimano,[1] Keiji Naruse,[4] Jun K. Yamashita,[5] Takashi Igarashi,[2] and Joji Ando[1]

[1]*Department of Biomedical Engineering and* [2]*Department of Pediatrics, Graduate School of Medicine, University of Tokyo, Tokyo, Japan;* [3]*PRESTO, Japan Science and Technology Agency, Saitama, Japan;* [4]*Department of Cardiovascular Physiology, Graduate School of Medicine, Dentistry, and Pharmaceutical Sciences, Okayama University, Okayama, Japan;* [5]*Stem Cell Research Center, Institute for Frontier Medical Sciences, Kyoto University, Kyoto, Japan*

Submitted 13 August 2007; accepted in final form 22 December 2007

Shimizu N, Yamamoto K, Obi S, Kumagaya S, Masumura T, Shimano Y, Naruse K, Yamashita JK, Igarashi T, Ando J. Cyclic strain induces mouse embryonic stem cell differentiation into vascular smooth muscle cells by activating PDGF receptor β. *J Appl Physiol* 104: 766–772, 2008. First published January 10, 2008; doi:10.1152/japplphysiol.00870.2007.—Embryonic stem (ES) cells are exposed to fluid-mechanical forces, such as cyclic strain and shear stress, during the process of embryonic development but much remains to be elucidated concerning the role of fluid-mechanical forces in ES cell differentiation. Here, we show that cyclic strain induces vascular smooth muscle cell (VSMC) differentiation in murine ES cells. Flk-1-positive (Flk-1$^+$) ES cells seeded on flexible silicone membranes were subjected to controlled levels of cyclic strain and examined for changes in cell proliferation and expression of various cell lineage markers. When exposed to cyclic strain (4–12% strain, 1 Hz, 24 h), the Flk-1$^+$ ES cells significantly increased in cell number and became oriented perpendicular to the direction of strain. There were dose-dependent increases in the VSMC markers smooth muscle α-actin and smooth muscle-myosin heavy chain at both the protein and gene expression level in response to cyclic strain, whereas expression of the vascular endothelial cell marker Flk-1 decreased, and there were no changes in the other endothelial cell markers (Flt-1, VE-cadherin, and platelet endothelial cell adhesion molecule 1), the blood cell marker CD3, or the epithelial marker keratin. The PDGF receptor β (PDGFRβ) kinase inhibitor AG-1296 completely blocked the cyclic strain-induced increase in cell number and VSMC marker expression. Cyclic strain immediately caused phosphorylation of PDGFRβ in a dose-dependent manner, but neutralizing antibody against PDGF-BB did not block the PDGFRβ phosphorylation. These results suggest that cyclic strain activates PDGFRβ in a ligand-independent manner and that the activation plays a critical role in VSMC differentiation from Flk-1$^+$ ES cells.

hemodynamic force; biomechanics; blood vessel

EMBRYONIC STEM (ES) cells derived from the inner cell mass of a blastocyst stage embryo are able to differentiate into the three embryonic germ layers (endoderm, ectoderm, and mesoderm) and are thus able to produce virtually all types of somatic cells (5, 16). ES cells are considered a promising source of seed cells for tissue engineering (22), and a great effort has been made to develop methods of inducing ES cells to differentiate into various specialized cells (1, 14, 25, 31). Yamashita et al. (34) developed a method that uses cell growth factors to induce selective differentiation of ES cells into vascular cells. In this method, undifferentiated mouse ES cells are cultured on type IV collagen-coated dishes, and vascular endothelial growth factor (VEGF) receptor 2 (Flk-1)-positive (Flk-1$^+$) cells are isolated by flow cytometry sorting. Addition of VEGF to the cultures promotes endothelial differentiation, whereas mural cells, including vascular smooth muscle cells (VSMCs) and pericytes, are induced by platelet-derived growth factor-BB (PDGF-BB). The vascular cells derived from Flk-1$^+$ cells have been shown to contribute to the developing vasculature in vivo.

Adult blood vessel cells are known to alter their shape, function, and gene expression in response to fluid-mechanical forces, such as shear stress produced by flowing blood and cyclic strain generated by pulsatile changes in blood pressure (3). The vascular cell responses to mechanical forces are thought to play an important role in sustaining the homeostasis of the circulatory system and in blood flow-dependent phenomena, such as angiogenesis, vascular remodeling, and atherogenesis. Fluid-mechanical forces have recently been shown to control embryonic development and organogenesis: intracardiac fluid forces are essential for the formation of a functional heart in zebrafish embryos (7), and the direction of fluid flow on the node of mouse embryos determines left-right asymmetry in the body plan (19). Moreover, it is now clear that fluid-mechanical forces affect immature and undifferentiated cells, as well as adult cells. Our previous studies (32, 33) showed that shear stress induces selective differentiation by bone marrow-derived endothelial progenitor cells and Flk-1$^+$ ES cells into the vascular endothelial cell (EC) lineage in vitro.

The hemodynamics of the mammalian embryo has recently been analyzed. Jones et al. (10, 11) made quantitative flow measurements during early organogenesis in mouse embryos and detected laminar shear stress levels of between 0 and 5.5 dyn/cm^2 in embryos from 8.5 to 10.5 days postcoitum (dpc) and a heart rate ranging from about 80 to 100 beats/min. According to data obtained from rat and chick embryos, pressure levels in embryos are low, ~1–2 mmHg (8, 17). During the process of embryonic development, ES cells appear to be exposed to shear stress and cyclic strain generated by the beating heart. Cyclic strain and shear stress have both been recognized as important modulators of vascular cell function, including cell proliferation, apoptosis, differentiation, morphology, migration, and the secretion of various macromolecules (12). More recent studies have revealed that cyclic strain

* N. Shimizu and K. Yamamoto contributed equally to this work.

Address for reprint requests and other correspondence: J. Ando, Dept. of Biomedical Engineering, Graduate School of Medicine, Univ. of Tokyo, 7-3-1 Hongo, Bunkyo-ku, Tokyo 113-0033, Japan (e-mail: joji@m.u-tokyo.ac.jp).

The costs of publication of this article were defrayed in part by the payment of page charges. The article must therefore be hereby marked "*advertisement*" in accordance with 18 U.S.C. Section 1734 solely to indicate this fact.

affects ES cell differentiation. Schmelter et al. (28) demonstrated that static mechanical strain promotes cardiovascular differentiation by ES cells through the generation of reactive oxygen species. Saha et al. (26), on the other hand, showed that mechanical strain has an inhibitory effect on ES cell differentiation. Thus the role of fluid-mechanical forces in ES cell differentiation seems open to discussion.

In the present study, we investigated whether cyclic strain affects the differentiation of Flk-1$^+$ ES cell and, if so, which cell lineage they differentiate into. Mouse Flk-1$^+$ ES cells cultured on flexible silicone membranes were subjected to controlled levels of cyclic strain and examined for changes in the expression of various cell lineage markers. We also investigated the molecular mechanism involved in the effects of cyclic strain on Flk-1$^+$ ES cell differentiation in terms of PDGF receptor phosphorylation.

MATERIALS AND METHODS

Cell culture. MGZ5 ES cells [gift from H. Niwa (Riken, CDB, Kobe, Japan)] were maintained, differentiated, and cultured as previously described (32). The cells were initially maintained undifferentiated without a feeder layer on gelatin-coated tissue culture dishes in DMEM (IBL, Fujioka, Japan) containing 15% FBS (JRH Biosciences), 10^3 U/ml leukemia inhibitory factor (ESGRO Complete kit; Chemicon), 1× nonessential amino acid (ICN Pharmaceuticals), and 5×10^{-5} mol/l β-mercaptoethanol (Sigma). To initiate ES cell differentiation, trypsinized cells were plated on type IV collagen-coated Petri dishes (BD Falcon) and cultured without leukemia inhibitory factor in α-MEM (GIBCO) containing 10% FBS, 50 U/ml penicillin-streptomycin (ICN Pharmaceuticals), and 5×10^{-5} mol/l β-mercaptoethanol. On *day 4*, Flk-1$^+$ ES cells were isolated by standard immunomagnetic techniques (MACS kit; Miltenyi Biotech) using anti-mouse Flk-1 antibody (Clone Avas 12α1; Pharmingen) and plated in differentiation medium (α-MEM containing 10% FBS, 50 U/ml penicillin-streptomycin, and 5×10^{-5} mol/l β-mercaptoethanol) in silicon chambers. After culture for 3 days, cells became confluent and were used for experiments.

Cyclic strain experiments. Flk-1$^+$ ES cells were exposed to cyclic strain with a uniaxial mechanical strain-loading device, as described previously (30). Briefly, type IV collagen-coated polydimethylsiloxane chambers in which the cells were cultured were fixed in a cyclic strain-loading device (STREX ST-140; Strex, Osaka, Japan). One end of the chamber was firmly attached to the fixed frame, and the other end of the chamber was fixed to the movable frame connected to a motor-driven shaft. The amplitude and frequency of stretching were controlled by a programmable microcomputer, and cyclic strain in the 2–12% range with 1 Hz was used in the present study. The polydimethylsiloxane membrane (32 mm × 32 mm) was uniaxially and uniformly stretched over the entire membrane area, except at both lateral edges (2–3 mm in width), where the strain was slightly lower than the amount applied; i.e., the difference between the lateral edges and other areas was no more than one-tenth of that applied. All experiments were performed at 37°C in a CO_2 incubator.

Immunohistochemistry. Cells were fixed with 4% paraformaldehyde (Sigma), permeabilized with 0.1% Triton X-100 (Sigma), and maintained in 1% normal BSA (Sigma) to block nonspecific protein binding sites. The cells were incubated with monoclonal antibodies against platelet endothelial cell adhesion molecule 1 (PECAM-1; Pharmingen) and then with monoclonal antibody against smooth muscle α-actin (SM α-actin; Sigma). After they were washed, cells were incubated with a secondary antibody (Alexa Fluor 488 goat anti-rat IgG or Alexa Fluor 594 goat anti-mouse IgG; Molecular Probes) at a dilution of 1:500. The cell nuclei were stained with 4′,6-diamidino-2-phenylindole (Sigma). Stained cells were photographed through a confocal laser scanning microscope (Leica), and all images were imported into Adobe Photoshop as JPEGs for contrast manipulation and figure assembly.

Western blot analysis. Western blot analyses were performed as previously described (32). Briefly, cells were dissolved in lysis buffer containing a 0.1% protease inhibitor mixture (Sigma) and centrifuged at 2.6×10^4 *g* for 30 min. The protein concentration of the lysate was determined with a protein assay kit (Bio-Rad). Equal amounts of protein were dissolved in SDS-PAGE sample buffer, separated by SDS-PAGE, transferred to Immobilon membranes (Millipore), and incubated with antibodies against SM α-actin or smooth muscle myosin heavy chain (SM-MHC; Biomedical Technologies). Anti-mouse PDGF receptor β (PDGFRβ) phosphospecific antibody (pY857; BD Pharmingen) was used for the analysis of PDGFRβ phosphorylation. After they were washed and incubated with horseradish peroxidase-linked anti-mouse or anti-rabbit IgG, immunoreactive proteins were visualized with the enhanced chemiluminescence plus detection system (Amersham) and GS363 molecular imager system (Bio-Rad).

Flow cytometry. Expression of various cell lineage marker proteins was measured by flow cytometry. Cells were detached from the dishes by incubation at room temperature for 15 min in PBS supplemented with 1 mM EDTA (Sigma) and then suspended in PBS with 10% FBS. A total of 200,000 cells were then incubated for 60 min at 4°C with monoclonal antibodies against the EC markers, including the VEGF receptors Flk-1 (Pharmingen) and Flt-1 (Chemicon), and the intercellular adhesion molecules VE-cadherin (Pharmingen) and PECAM-1, the blood cell marker T3 antigen (CD3; Pharmingen), and the epithelial cell marker keratin (NeoMarkers). Next, the cells were incubated for 60 min at 4°C with Alexa Fluor 488 goat anti-mouse IgG (Molecular Probes) and analyzed by fluorescence-activated cell sorting (Becton Dickinson). Histograms of cell number vs. logarithmic fluorescence intensity were recorded for 20,000 cells per sample. Background fluorescence was obtained from the negative control cells stained with the secondary antibody and subtracted from the mean fluorescence of the specific staining patterns. The expression level of each antigen was expressed as the mean channel fluorescence.

Real-time PCR analysis. Total RNA samples were prepared from cells with ISOGEN (Nippon Gene, Tokyo, Japan), and first-strand cDNAs were generated by using Moloney murine leukemia virus reverse transcriptase (Roche) and RNA primed with oligo(dT) primer. After reverse transcription of the RNA into cDNA, real-time PCR was used to monitor gene expression with a Smart Cycler (Cepheid) according to the standard procedure. PCR was performed with a Takara EX *Taq* R-PCR version (Takara) and the primer pairs shown in Table 1. The temperature profile consisted of initial denaturation for 30 s at 95°C followed by 35 cycles of denaturation at 95°C for 15 s, annealing at 60°C for 15 s, elongation at 72°C, and fluorescence monitoring at 85°C. The specificity of the amplification reaction was determined by performing a melting-curve analysis. Relative quantification of the signals was achieved by normalizing the signals of the different genes to β-actin.

Statistical analysis. All data are expressed as means ± SD. Statistical significance was evaluated by an ANOVA and a Bonferonni's adjustment applied to the results of a *t*-test with software from SPSS. A P value of <0.05 was regarded as statistically significant.

RESULTS

Cyclic strain enhances Flk-1$^+$ ES cell proliferation. The same number of Flk-1$^+$ ES cells were plated in silicon chambers; after the cells became confluent, they were subjected to cyclic strain (4, 8, or 12% strain, 1 Hz) or incubated under static conditions for 24 h. The cells were removed by trypsinization, and a Coulter counter was used to count their number (Fig. 1*A*). Cell number increased in response to cyclic strain, peaked at 8% strain, and leveled off at 12% strain. The

Table 1. *Oligonucleotide primers used for real-time PCR*

Gene	Primer Sequence	Amplified Fragment Size, bp
SM α-actin	Fwd: 5′-ACGGCCGCCTCCTCTTCCTC-3′ Rev: 5′-GCCCAGCTTCGTCGTATTCC-3′	415
SM-MHC	Fwd: 5′-GACAACTCCTCTCGCTTTGG-3′ Rev: 5′-GCTCTCCAAAAGCAGGTCAC-3′	201
SM22α	Fwd: 5′-GCAGTCCAAAATTGAGAAGA-3′ Rev: 5′-CTGTTGCTGCCCATTTGAAG-3′	507
Flk-1	Fwd: 5′-TCTGTGGTTCTGCGTGGAGA-3′ Rev: 5′-GTATCATTTCCAACGACCCT-3′	248
Flt-1	Fwd: 5′-CGGAAGCTCTGATGATGTGA-3′ Rev: 5′-TATCTTCATGGAGGCCTTGG-3′	199
VE-cadherin	Fwd: 5′-CTTCCGAATAACCAAGCAGG-3′ Rev: 5′-TACTTGACCGTGATGTTGGC-3′	369
PECAM-1	Fwd: 5′-ACATGCCATAGGCATCAGC-3′ Rev: 5′-TCACAGAGCACCGAAGTACC-3′	305
β-Actin	Fwd: 5′-GTCGTACCACAGGCATTGTGATGG-3′ Rev: 5′-GCAATGCCTGGGTGCATGGTGG-3′	493

Fwd, forward; Rev, reverse; SM, smooth muscle; MHC, myosin heavy chain; PECAM-1, platelet endothelial cell adhesion molecule-1.

increase in cell number at 8% or 12% strain was almost the same as the level induced by a maximally effective concentration of PDGF-BB (23). Flk-1$^+$ ES cells were subjected to cyclic strain (8% strain, 1 Hz) in the presence of the PDGF receptor kinase inhibitor AG-1296, which potently and selectively inhibits signaling of PDGFRα and PDGFRβ as well as of its family member *Kit* (13). AG-1296 almost completely suppressed the cyclic strain-induced increase in cell number, indicating that PDGF receptor activation is involved in the effect of cyclic strain on Flk-1$^+$ ES cell proliferation.

Flk-1$^+$ ES cells that had been cultured under static conditions or that had been exposed to cyclic strain (8%, 1 Hz) or PDGF-BB for 24 h were immunostained for an EC marker, PECAM-1, and a VSMC marker, SM α-actin (Fig. 1*B*). Under static conditions, most of the cells stained positive for SM α-actin (red) and some of the cells stained positive for PECAM-1 (green). When exposed to cyclic strain, the number of PECAM-1-positive cells decreased, whereas the number of SM α-actin-positive cells increased, and their long axis became oriented perpendicular to the direction of strain. Addition of PDGF-BB also decreased the number of PECAM-1-positive cells and increased the number of SM α-actin-positive cells, but it did not cause any change in cell orientation. The percentage of PECAM-1-positive cells determined by flow cytometry was 12.3 ± 0.25% (mean ± SD, $n = 5$) of the static control cells, 2.41 ± 0.35% of the cells exposed to cyclic strain ($P < 0.01$ vs. static control), and 3.25 ± 0.24% of the cells treated with PDGF-BB ($P < 0.01$ vs. static control).

Cyclic strain induces differentiation of Flk-1$^+$ ES cells into the VSMC lineage. Flk-1$^+$ ES cells that had been cultured under static conditions or exposed to cyclic strain (2, 4, 8, or 12%, 1 Hz) for 24 h were examined for changes in expression of various cell lineage markers. When exposed to cyclic strain, expression of the VSMC markers SM α-actin and SM-MHC increased markedly in a dose-dependent manner (Fig. 2, *A* and *B*). By contrast, cyclic strain (8%, 1 Hz, 24 h) significantly decreased the expression of the EC marker Flk-1 and had no effect on the expression of the other EC markers (Flt-1, VE-cadherin, and PECAM-1), the blood cell marker CD3, or the epithelial marker keratin (Fig. 2*C*). The addition of PDGF-BB to static Flk-1$^+$ ES cells had almost the same

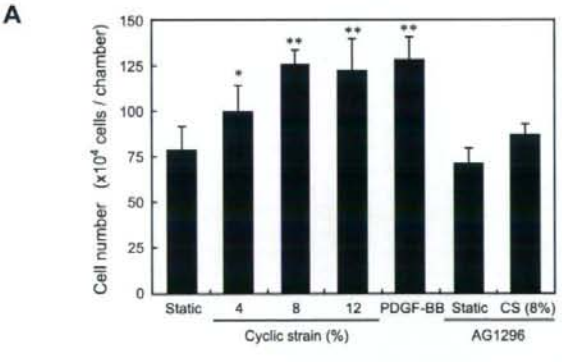

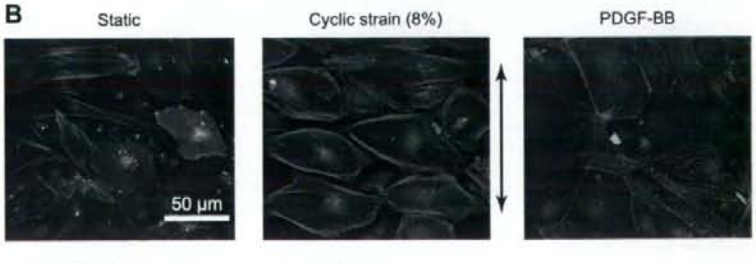

Fig. 1. Effect of cyclic strain on cell proliferation and differentiation. *A*: cell number of Flk-1-positive (Flk-1$^+$) embryonic stem (ES) cells cultured under static conditions or exposed to cyclic strain (4, 8, or 12% strain, 1 Hz) or PDGF-BB (10 ng/ml) for 24 h. Cell number increased in response to cyclic strain. The PDGF receptor β (PDGFRβ) kinase inhibitor AG-1296 (10 μmol/l) blocked the cell proliferation-promoting effect of cyclic strain. CS, cyclic strain. Values are means ± SD of data from 5 separate cell samples. *$P < 0.05$ and **$P < 0.01$ vs. static control. *B*: photomicrographs of immunostained Flk-1$^+$ ES cells cultured under static conditions or exposed to cyclic strain (8%, 1 Hz) or to PDGF-BB (10 ng/ml) for 24 h. Cells were immunostained for the endothelial cell (EC) marker platelet endothelial cell adhesion molecule 1 [PECAM-1 (green)] and a vascular smooth muscle cell (VSMC) marker [smooth muscle (SM) α-actin (red)]. The cell nuclei were stained with 4′,6-diamidino-2-phenylindole (blue). Cyclic strain and PDGF-BB increased SM α-actin-positive cells, whereas they decreased PECAM-1-positive cells. Under cyclic strain, SM α-actin-positive cells aligned themselves perpendicular to the direction of the strain. The direction of strain is from *top* to *bottom* (arrow).

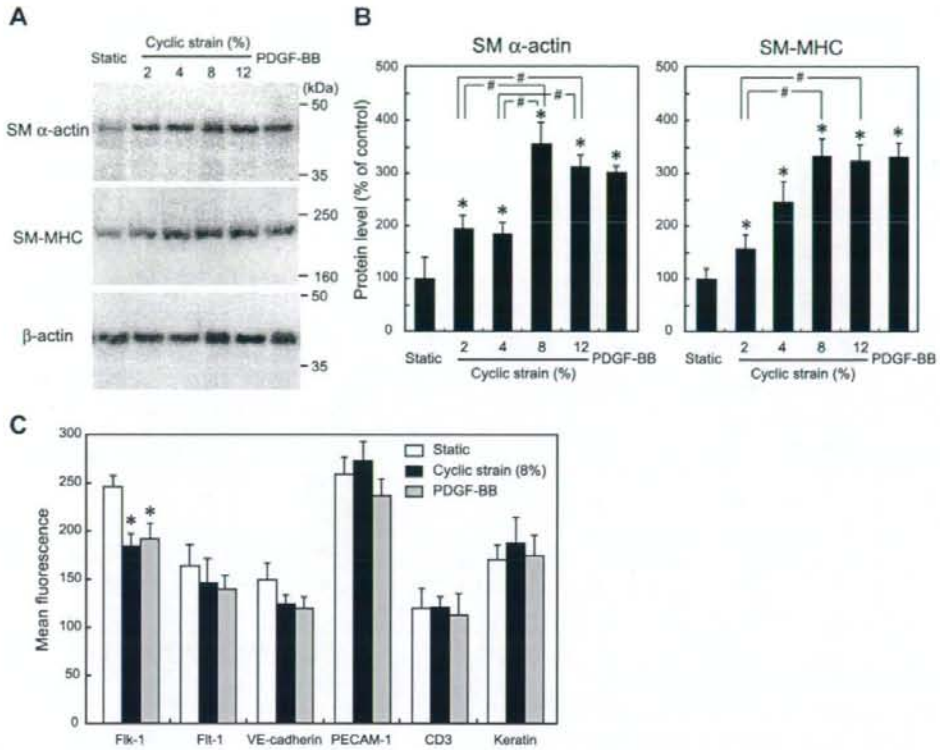

Fig. 2. Effect of cyclic strain on expression of various cell lineage marker proteins. *A*: visualization of bands of the VSMC markers SM α-actin and smooth muscle myosin heavy chain (SM-MHC). Total protein was isolated from Flk-1$^+$ ES cells cultured under static conditions or exposed to cyclic strain (2, 4, 8, and 12%, 1 Hz) or to PDGF-BB (10 ng/ml) for 24 h. After electrophoresis and transfer to a PVDF membrane, the protein was immunoblotted with specific antibody to SM α-actin, SM-MHC, or the cytoskeletal protein β-actin, which was used as a protein loading control. *B*: relative protein levels of SM α-actin and SM-MHC. Cyclic strain dose dependently increased protein expression of both SM α-actin and SM-MHC. Values are means ± SD of 5 different experiments. *$P < 0.01$ vs. static control. #$P < 0.01$ between the cells exposed to 2% and 4% strain and those exposed to 8% and 12% strain. *C*: relative protein levels of the EC markers Flk-1, Flt-1, VE-cadherin, and PECAM-1, the blood cell marker CD3, and the epithelial marker keratin. After exposure to cyclic strain (8%, 1 Hz) or PDGF-BB (10 ng/ml) for 24 h, cells were immunostained with specific antibody against each marker and examined for changes in cell surface expression by flow cytometry. Cyclic strain decreased protein expression of Flk-1 but had no effect on expression of Flt-1, VE-cadherin, PECAM-1, CD3, or keratin. Exposure to PDGF-BB had the same effect as cyclic strain. Values are means ± SD of 4 separate samples. *$P < 0.01$ vs. static control.

effect on expression of these cell lineage marker proteins as 8% strain did.

Gene expression of cell lineage markers was examined by real-time PCR. Cyclic strain markedly increased the mRNA levels of the VSMC markers SM α-actin, SM-MHC, and smooth muscle 22α in a dose-dependent manner (Fig. 3*A*). By contrast, the Flk-1 mRNA levels decreased in response to cyclic strain (8%, 1 Hz), but the mRNA levels of Flt-1, VE-cadherin, and PECAM-1 remained unchanged (Fig. 3*B*). Together, these results indicate that cyclic strain selectively promotes differentiation of Flk-1$^+$ ES cells into VSMCs but not into the EC, blood cell, or epithelial cell lineages.

PDGFRβ is involved in the cyclic strain-induced differentiation of Flk-1$^+$ ES cells. Flk-1$^+$ ES cells were subjected to cyclic strain (8%,1 Hz) for 24 h in the presence or absence of AG-1296 and examined for changes in the expression of SM α-actin and SM-MHC proteins. Cyclic strain markedly increased the expression of SM α-actin and SM-MHC in the absence of AG-1296 but not in its presence (Fig. 4). AG-1296 decreased the basal levels of SM α-actin and SM-MHC, indicating that a slight degree of PDGF receptor phosphorylation occurs even under static conditions. AG-1296 seems to have inhibited both basal and cyclic-strain-induced PDGF receptor phosphorylation. These findings suggest that PDGFRβ activation plays an important role in the cyclic strain-induced VSMC differentiation from Flk-1$^+$ ES cells.

Cyclic strain activates PDGFRβ in a ligand-independent manner. Because the experiments with AG-1296 showed the involvement of PDGFRβ activation in cyclic-strain-induced ES cell differentiation, we investigated whether cyclic strain causes PDGFRβ activation. When Flk-1$^+$ ES cells were exposed to PDGF-BB or cyclic strain, phosphorylation of PDGFRβ occurred within 10 min but was almost completely blocked by AG-1296 (Fig. 5*A*). The cyclic strain-induced PDGFRβ phosphorylation was dose dependent (Fig. 5*B*). Neither neutralizing antibody against PDGF-BB nor against VEGF inhibited the cyclic strain-induced PDGFRβ phosphorylation (Fig. 5*C*). To investigate whether a ligand released by the cells was involved in the

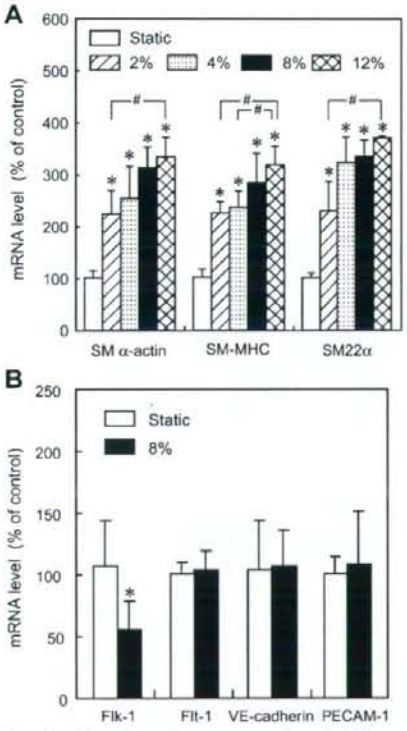

Fig. 3. Effect of cyclic strain on the gene expression of cell lineage markers. Flk-1$^+$ ES cells were exposed to cyclic strain (2, 4, 8, and 12% strain, 1 Hz) for 24 h and examined for changes in gene expression by real-time PCR. *A*: changes in the mRNA levels of VSMC markers. Cyclic strain increased the mRNA levels of SM α-actin, SM-MHC, and smooth muscle 22α (SM22α) in a dose-dependent manner. Values are means ± SD of 3 cell samples. *$P <$ 0.01 vs. static control. #$P < 0.01$ between the cells exposed to 2% and 4% strain and those exposed to 8% and 12%. *B*: changes in the mRNA levels of the EC markers Flk-1, Flt-1, VE-cadherin, and PECAM-1. Cyclic strain (8%, 1 Hz, 24 h) decreased the mRNA level of Flk-1 but had no effect on the mRNA level of Flt-1, VE-cadherin, or PECAM-1. Values are means ± SD of 6 cell samples. *$P < 0.01$ vs. static control.

PDGFRβ activation, Flk-1$^+$ ES cells were exposed to conditioned medium obtained from cells exposed to cyclic strain (8%, 1 Hz) for 10 min. However, the conditioned medium did not induce PDGFRβ phosphorylation, and the extracellular ATP scavenger apyrase, the G protein-coupled receptor inhibitor pertussis toxin, and depletion of extracellular Ca^{2+} were incapable of attenuating the PDGFRβ phosphorylation. These results indicate that cyclic strain causes PDGFRβ phosphorylation in a ligand-independent manner and that transactivation of PDGFRβ secondary to activation of ATP receptors or G-protein-coupled receptors or Ca^{2+} influx via ion channels is not involved in the cyclic strain-induced PDGFRβ phosphorylation.

DISCUSSION

The results of this study demonstrated that cyclic strain significantly promotes the proliferation of Flk-1$^+$ ES cells and increases the expression of SM α-actin, SM-MHC, and smooth muscle 22α, which are markers of a differentiated VSMC phenotype (20). Upregulation of VSMC markers by cyclic strain has been observed in other immature cell lines, such as rat bone marrow progenitor cells (6), human bone marrow mesenchymal stem cells (21), and murine embryonic mesenchymal progenitor cells (24). However, this study showed that cyclic strain decreases the expression of Flk-1 but has no effect on the expression of other EC markers, including Flt-1, VE-cadherin, and PECAM-1, the blood cell marker CD3, or the epithelial cell marker keratin. These findings suggest that cyclic strain induces selective differentiation of Flk-1$^+$ ES cells into the VSMC lineage and not into other cell lineages. Our previous study showed that shear stress induces endothelial differentiation by Flk-1$^+$ ES cells, indicating that shear stress and cyclic strain have very different effects on ES cell differentiation (32). It therefore appears that shear stress may inhibit a pathway that leads to ES cell differentiation into smooth muscle cells and that cyclic strain may inhibit a pathway that leads to ES cell differentiation into ECs. Because, under in vivo conditions, ES cells seem to be exposed to both cyclic strain and shear stress, to understand the roles of fluid-mechanical forces in cardiovascular differentiation and devel-

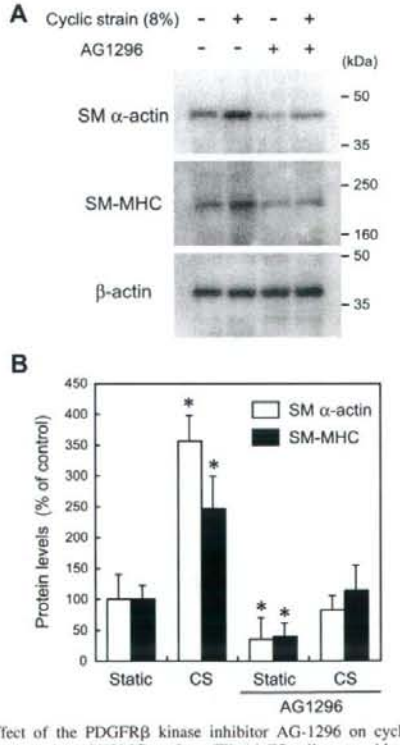

Fig. 4. Effect of the PDGFRβ kinase inhibitor AG-1296 on cyclic strain-induced upregulation of VSMC markers. Flk-1$^+$ ES cells were either cultured under static conditions or exposed to cyclic strain (8%, 1 Hz) for 24 h in the absence or presence of AG-1296 (10 μmol/l). *A*: visualization of bands of SM α-actin, SM-MHC, and β-actin (used as a protein loading control). *B*: histograms of the relative protein levels of SM α-actin and SM-MHC. Cyclic strain (CS) increased protein expression of both SM α-actin and SM-MHC, and AG-1296 almost completely abolished the effects of cyclic strain. Values are means ± SD of 4 cell samples. *$P < 0.01$ vs. static control.

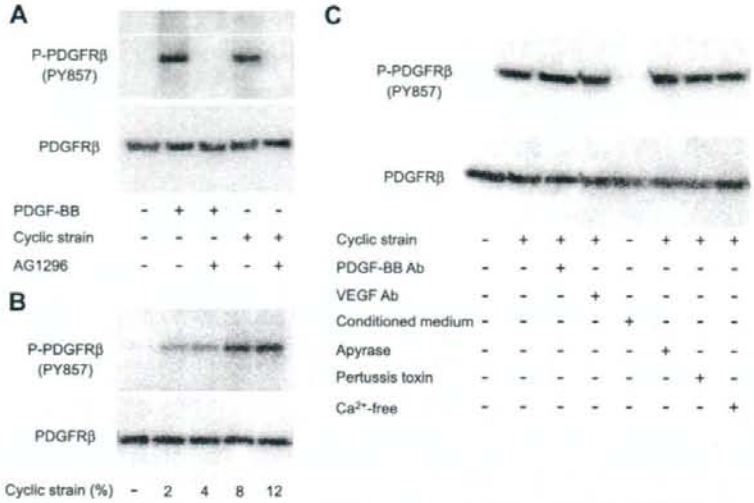

Fig. 5. Effect of cyclic strain on PDGFRβ phosphorylation. *A*: cyclic strain-induced phosphorylation of PDGFRβ. Flk-1$^+$ ES cells were either cultured under static conditions or exposed to PDGF-BB (10 ng/ml) or cyclic strain (8%, 1 Hz) for 10 min. Tyrosine-phosphorylated proteins associated with anti-PDGFRβ (P-PDGFRβ) were detected by immunoblotting with anti-phosphotyrosine antibody (PY-857). The total amount of PDGFRβ in cell lysates was also determined with anti-PDGFRβ antibody. Cyclic strain and PDGF-BB caused phosphorylation of PDGFRβ, and it was completely blocked by AG-1296 (10 μmol/l). Experiments were repeated 3 times, and similar results were obtained. *B*: dose dependency of cyclic strain-induced PDGFRβ phosphorylation. *C*: effects of various inhibitors on PDGFRβ phosphorylation. None of the neutralizing antibodies against PDGF-BB (1 μg/ml; R&D Systems), VEGF (1 μg/ml; R&D Systems), apyrase (20 U/ml; Sigma), or pertussis toxin (100 ng/ml; Sigma) attenuated the cyclic strain-induced PDGFRβ phosphorylation. Addition of conditioned medium obtained from Flk-1$^+$ ES cells exposed to cyclic strain (8%, 1 Hz) for 10 min did not cause PDGFRβ phosphorylation. Cyclic strain caused PDGFRβ phosphorylation even after the incubation for 10 min in Ca^{2+}-free HBSS with EGTA (2 mM). Experiments were repeated 3 times, with similar results.

opment in embryo it will be necessary to know the ES cell responses, not only to cyclic strain alone and to shear stress alone but to combinations of the two.

The upregulation of Flk-1$^+$ ES cell proliferation and expression of VSMC markers by cyclic strain were almost completely blocked by the PDGFRβ kinase inhibitor AG-1296, suggesting that PDGFRβ activation plays an important role in the effects of cyclic strain. Western blot analysis revealed that phosphorylation of PDGFRβ occurs immediately after the application of cyclic strain to Flk-1$^+$ ES cells. Because cyclic strain has been shown to cause mature ECs and VSMCs to release PDGF-BB, which is the ligand for PDGFRβ (15, 29), we investigated whether Flk-1$^+$ ES cells release PDGF-BB in response to cyclic strain. The concentration of PDGF-BB in the conditioned medium obtained from the cells exposed to cyclic strain for 10 min was below the limits of detection by ELISA (data not shown), indicating that very little, if any, PDGF-BB release occurred shortly after the onset of cyclic strain. However, because autocrine systems can be active even when no ligands are found in the extracellular medium (4), it is impossible to rule out the possibility based on the results of ELISA that a small amount of PDGF-BB is elicited by cyclic strain and that it acts on adjacent neighbor cells in a highly localized manner as an autocrine or paracrine signal. It was recently reported that VEGF-A binds and activates PDGFRα and PDGFRβ in bone marrow-derived human adult mesenchymal stem cells (2). However, neutralizing antibody specific to PDGF-BB and VEGF did not block the cyclic strain-induced PDGFRβ phosphorylation. In addition, phosphorylation of PDGFRβ did not occur when Flk-1$^+$ ES cells were exposed to conditioned medium obtained from the cells subjected to cyclic strain for 10 min. From the above findings, the phosphorylation of PDGFRβ induced by cyclic strain does not seem to involve any ligands, including PDGF or VEGF.

The ligand-independent activation of PDGFRβ by cyclic strain seen in Flk-1$^+$ ES cells is analogous to that observed in adult VSMCs (9). Cyclic strain rapidly induced phosphorylation of PDGFRα in VSMCs, but neither antibodies that bind to all forms of PDGFs nor conditioned medium from VSMCs exposed to cyclic strain blocked cyclic strain-induced PDGFRα activation. It is unclear, however, how cyclic strain activates PDGF receptor in a ligand-independent manner. The following possibilities can be considered. *1*) Cyclic strain mechanically deforms the cell membrane, which may influence PDGF receptor conformation or dimerization, and lead to its phosphorylation. *2*) Other molecules besides PDGF receptor, including other receptors, ion channels, and integrins, may transduce the mechanical stress into chemical signals and lead to PDGF receptor activation via a cross-talking mechanism. This study did not cover the involvement of stretch-activated ion channels or integrins, both of which are known to function as mechanotransducers (18, 27), but the results showed that apyrase, pertussis toxin, and depletion of extracellular Ca^{2+} had no effect on cyclic-strain-induced PDGFRβ activation. These findings suggest that PDGFRβ was not transactivated, at least not via ATP receptors, G protein-coupled receptors, or Ca^{2+} influx. Interestingly, our previous study (32) revealed that shear stress activates Flk-1 in a ligand-independent manner and that the activation of Flk-1 plays a critical role in endothelial differentiation of Flk-1$^+$ ES cells. Thus cyclic strain and shear stress may act by

a common mechanism in which growth factor receptors are activated by mechanical forces without ligand binding. Elucidation of the mechanism would lead to a better understanding of mechanotransduction and its role in ES cell differentiation.

ACKNOWLEDGMENTS

The authors thank Yuko Sawada for technical assistance.

GRANTS

This study was supported in part by Grants-in-Aid for Scientific Research on Priority Areas and from the Ministry of Education, Culture, Sports, Science, and Technology and by a research grant for cardiovascular diseases from the Japanese Ministry of Health, Labor, and Welfare.

REFERENCES

1. **Bain G, Kitchens D, Yao M, Huettner JE, Gottlieb DI.** Embryonic stem cells express neuronal properties in vitro. *Dev Biol* 168: 342–357, 1995.
2. **Ball SG, Shuttleworth CA, Kielty CM.** Vascular endothelial growth factor can signal through platelet-derived growth factor receptors. *J Cell Biol* 177: 489–500, 2007.
3. **Davies PF.** Flow-mediated endothelial mechanotransduction. *Physiol Rev* 75: 519–560, 1995.
4. **DeWitt AE, Dong JY, Wiley HS, Lauffenburger DA.** Quantitative analysis of the EGF receptor autocrine system reveals cryptic regulation of cell response by ligand capture. *J Cell Sci* 114: 2301–2313, 2001.
5. **Evans MJ, Kaufman MH.** Establishment in culture of pluripotential cells from mouse embryos. *Nature* 292: 154–156, 1981.
6. **Hamilton DW, Maul TM, Vorp DA.** Characterization of the response of bone marrow-derived progenitor cells to cyclic strain: implications for vascular tissue-engineering applications. *Tissue Eng* 10: 361–369, 2004.
7. **Hove JR, Koster RW, Forouhar AS, Acevedo-Bolton G, Fraser SE, Gharib M.** Intracardiac fluid forces are an essential epigenetic factor for embryonic cardiogenesis. *Nature* 421: 172–177, 2003.
8. **Hu N, Clark EB.** Hemodynamics of the stage 12 to stage 29 chick embryo. *Circ Res* 65: 1665–1670, 1989.
9. **Hu Y, Bock G, Wick G, Xu Q.** Activation of PDGF receptor α in vascular smooth muscle cells by mechanical stress. *FASEB J* 12: 1135–1142, 1998.
10. **Jones EA, Baron MH, Fraser SE, Dickinson ME.** Measuring hemodynamic changes during mammalian development. *Am J Physiol Heart Circ Physiol* 287: H1561–H1569, 2004.
11. **Jones EA, Crotty D, Kulesa PM, Waters CW, Baron MH, Fraser SE, Dickinson ME.** Dynamic in vivo imaging of postimplantation mammalian embryos using whole embryo culture. *Genesis* 34: 228–235, 2002.
12. **Kakisis JD, Liapis CD, Sumpio BE.** Effects of cyclic strain on vascular cells. *Endothelium* 11: 17–28, 2004.
13. **Kovalenko M, Gazit A, Bohmer A, Rorsman C, Ronnstrand L, Heldin CH, Waltenberger J, Bohmer FD, Levitzki A.** Selective platelet-derived growth factor receptor kinase blockers reverse sis-transformation. *Cancer Res* 54: 6106–6114, 1994.
14. **Kramer J, Hegert C, Guan K, Wobus AM, Muller PK, Rohwedel J.** Embryonic stem cell-derived chondrogenic differentiation in vitro: activation by BMP-2 and BMP-4. *Mech Dev* 92: 193–205, 2000.
15. **Ma YH, Ling S, Ives HE.** Mechanical strain increases PDGF-B and PDGF beta receptor expression in vascular smooth muscle cells. *Biochem Biophys Res Commun* 265: 606–610, 1999.
16. **Martin GR.** Isolation of a pluripotent cell line from early mouse embryos cultured in medium conditioned by teratocarcinoma stem cells. *Proc Natl Acad Sci USA* 78: 7634–7638, 1981.
17. **Nakazawa M, Morishima M, Tomita H, Tomita SM, Kajio F.** Hemodynamics and ventricular function in the day-12 rat embryo: basic characteristics and the responses to cardiovascular drugs. *Pediatr Res* 37: 117–123, 1995.
18. **Naruse K, Yamada T, Sokabe M.** Involvement of SA channels in orienting response of cultured endothelial cells to cyclic stretch. *Am J Physiol Heart Circ Physiol* 274: H1532–H1538, 1998.
19. **Nonaka S, Shiratori H, Saijoh Y, Hamada H.** Determination of left-right patterning of the mouse embryo by artificial nodal flow. *Nature* 418: 96–99, 2002.
20. **Owens GK.** Regulation of differentiation of vascular smooth muscle cells. *Physiol Rev* 75: 487–517, 1995.
21. **Park JS, Chu JS, Cheng C, Chen F, Chen D, Li S.** Differential effects of equiaxial and uniaxial strain on mesenchymal stem cells. *Biotechnol Bioeng* 88: 359–368, 2004.
22. **Pedersen RA.** Embryonic stem cells for medicine. *Sci Am* 280: 68–73, 1999.
23. **Raines EW, Ross R.** Purification of human platelet-derived growth factor. *Methods Enzymol* 109: 749–773, 1985.
24. **Riha GM, Wang X, Wang H, Chai H, Mu H, Lin PH, Lumsden AB, Yao Q, Chen C.** Cyclic strain induces vascular smooth muscle cell differentiation from murine embryonic mesenchymal progenitor cells. *Surgery* 141: 394–402, 2007.
25. **Rohwedel J, Maltsev V, Bober E, Arnold HH, Hescheler J, Wobus AM.** Muscle cell differentiation of embryonic stem cells reflects myogenesis in vivo: developmentally regulated expression of myogenic determination genes and functional expression of ionic currents. *Dev Biol* 164: 87–101, 1994.
26. **Saha S, Ji L, de Pablo JJ, Palecek SP.** Inhibition of human embryonic stem cell differentiation by mechanical strain. *J Cell Physiol* 206: 126–137, 2006.
27. **Sasamoto A, Nagino M, Kobayashi S, Naruse K, Nimura Y, Sokabe M.** Mechanotransduction by integrin is essential for IL-6 secretion from endothelial cells in response to uniaxial continuous stretch. *Am J Physiol Cell Physiol* 288: C1012–C1022, 2005.
28. **Schmelter M, Ateghang B, Helmig S, Wartenberg M, Sauer H.** Embryonic stem cells utilize reactive oxygen species as transducers of mechanical strain-induced cardiovascular differentiation. *FASEB J* 20: 1182–1184, 2006.
29. **Sumpio BE, Du W, Galagher G, Wang X, Khachigian LM, Collins T, Gimbrone MA Jr, Resnick N.** Regulation of PDGF-B in endothelial cells exposed to cyclic strain. *Arterioscler Thromb Vasc Biol* 18: 349–355, 1998.
30. **Takeda H, Komori K, Nishikimi N, Nimura Y, Sokabe M, Naruse K.** Bi-phasic activation of eNOS in response to uni-axial cyclic stretch is mediated by differential mechanisms in BAECs. *Life Sci* 79: 233–239, 2006.
31. **Vittet D, Prandini MH, Berthier R, Schweitzer A, Martin-Sisteron H, Uzan G, Dejana E.** Embryonic stem cells differentiate in vitro to endothelial cells through successive maturation steps. *Blood* 88: 3424–3431, 1996.
32. **Yamamoto K, Sokabe T, Watabe T, Miyazono K, Yamashita JK, Obi S, Ohura N, Matsushita A, Kamiya A, Ando J.** Fluid shear stress induces differentiation of Flk-1-positive embryonic stem cells into vascular endothelial cells in vitro. *Am J Physiol Heart Circ Physiol* 288: H1915–H1924, 2005.
33. **Yamamoto K, Takahashi T, Asahara T, Ohura N, Sokabe T, Kamiya A, Ando J.** Proliferation, differentiation, and tube formation by endothelial progenitor cells in response to shear stress. *J Appl Physiol* 95: 2081–2088, 2003.
34. **Yamashita J, Itoh H, Hirashima M, Ogawa M, Nishikawa S, Yurugi T, Naito M, Nakao K, Nishikawa S.** Flk1-positive cells derived from embryonic stem cells serve as vascular progenitors. *Nature* 408: 92–96, 2000.

ES 細胞および iPS 細胞からの血管細胞分化

Vascular cell differentiation from ES and iPS cells

Keywords

ES 細胞 (Embryonic stem cells)
iPS 細胞(induced pluripotent stem cells)
分化
血管再生

山下 潤

京都大学再生医科学研究所 幹細胞分化制御研究領域

Summary

We have been investigating molecular mechanisms of vascular development and regeneration using embryonic stem (ES) cells. Previously, we established an ES cell differentiation system that reproduces early vascular development using vascular endothelial growth factor (VEGF) receptor-2 (Flk1) -positive cells as common vascular progenitors. Recently, we succeeded in inducing arterial, venous, and lymphatic endothelial cells (ECs) from ES cells. More recently, a novel pluripotent stem cell line, induced pluripotent stem (iPS) cells, was established from mouse and human somatic cells. We applied our ES cell differentiation system to mouse iPS cells, and succeeded in systematically inducing cardiovascular cells from iPS cells. Time course and efficiency of the mouse iPS cell differentiation were all comparable with those of mouse ES cells. This study would largely contribute to novel understanding for iPS cell biology and the development of novel cardiovascular regenerative medicine. Here I discuss perspectives for vascular biology and medicine using ES and iPS cells.

Yamashita, Jun K

Laboratory of Stem Cell Differentiation, Institute for Frontier Medical Sciences, Kyoto University

E-mail : juny@frontier.kyoto-u.ac.jp

はじめに

虚血性心疾患を中心とする心疾患および脳血管障害は日本における死因のそれぞれ第 2 位 (10 万対 126) と 3 位 (10 万対 102) を占め，両者を合わせると第 1 位の悪性新生物 (がん) (10 万対 254) に肉薄する。一方国民医療費では，虚血性心疾患と脳血管障害を合わせると悪性新生物を上回り (2 兆 5 千億 vs 2 兆 3 千億円) (以上厚生労働省「平成 16 年度国民医療費の概況」)，心血管系疾患は，現在および未来にわたり日本の医療が取り組むべき最重要研究課題の 1 つと考えられる。近年の幹細胞生物学の発展を背景とした再生医療研究において，血管および心臓は最も急速に研究の進展が認められる臓器である。すなわち，さまざまな新しい心血管幹細胞・前駆細胞の発見や心血管分化機構の解析，さらには前駆細胞をヒトに用いた再生医療の試みまで，

基礎研究から臨床応用に至る幅広い知見が蓄積されてきた。なかでも血管は，骨髄細胞や末梢血細胞の虚血組織への移植，という細胞移植治療がすでに臨床の場にも応用され成果をあげており，近年の再生医療の発展において先駆的役割を果たしている。本稿はその中で万能の幹細胞として期待されるES細胞および最近樹立された新しい多能性幹細胞iPS細胞の血管分化とその応用に関する知見を中心に概説する。

ES細胞由来血管前駆細胞とその分化

筆者らはES細胞由来VEGFR2（2型血管内皮増殖因子受容体；Flk1）陽性細胞が，血管を構成する細胞である血管内皮細胞と血管壁細胞（血管平滑筋細胞およびペリサイト）の共通の前駆細胞であり，VEGFR2陽性細胞から内皮細胞および壁細胞の双方が分化誘導でき，毛細血管様の高次構造を培養下に形成できることを示した[1]。VEGFR2陽性の血管前駆細胞は，VEGF（血管内皮増殖因子）の刺激により内皮細胞に，主にPDGF-BB（血小板由来増殖因子）により壁細胞に分化すると考えられる。また，血流による物理的刺激であるshearストレスや拍動性進展刺激がVEGFR2陽性細胞からの内皮細胞分化や壁細胞分化を誘導することも明らかにされている。

最近，動脈，静脈，リンパ管それぞれの内皮細胞特異的に発現している分子が数々報告され，内皮細胞の多様性に分子的根拠が与えられるようになってきた[2]。筆者らは最近，VEGFR2陽性細胞からの血管分化系を用い，ephrinB2陽性（動脈）内皮，ephrinB2陰性（静脈）内皮，およびprox-1陽性（リンパ管）内皮細胞と考えられる細胞の誘導と純化にそれぞれ成功した[3][4]。すなわち，VEGFR2陽性細胞をVEGFおよび血清存在下に内皮細胞に誘導するとほとんど（＞90～95％）の内皮細胞がephrinB2陰性の静脈内皮細胞となる。VEGFに加えて，cAMPアナログである8bromo-cAMPまたは細胞内cAMPを上昇させる液性因子の1つであるアドレノメデュリン（AM）を加えcAMP経路を活性化することにより，内皮細胞においてNotchシグナルの活性化が誘導され，ephrinB2陽性の動脈内皮細胞が誘導される。また一方，VEGFR2陽性細胞をOP9ストローマ細胞上で培養して内皮細胞を誘導したところ，prox-1陽性リンパ管内皮細胞が出現した。このOP9によるリンパ管誘導作用は，VEGF-CおよびangiopoietinのVEGFR3シグナルの作用をブロックすることによりほぼ完全に阻害された。これらの結果により，ES細胞を用いて，動脈，静脈，リンパ管内皮細胞のすべてを系統的に分化誘導することが可能になるとともにその新たな分化メカニズムが明らかになった[5]（図1）。こうした新たなアプローチで血管分化多様化機構を解析することにより，動脈特異的血管新生やリンパ管特異的新生抑制による抗癌治療などの開発も期待される。さらに詳細に臓器特異的な血管の多様性を解析し理解することは，血管を介した臓器機能や病態の理解とそれに基づくさまざまな新しい治療戦略の開拓に結びつくと考えられる。

ES細胞による血管再生

筆者らはES細胞由来細胞の血管再生治療応用における可能性を検討するため，ES細胞由来血管細胞の成体に対する移植効果を検討した[6]。すなわち，ES細胞由来血管細胞をヌードマウスに移植した腫瘍周囲に注入し，移植細胞の新生血管への寄与を検討したところ，ES細胞由来VEGFR2陽性細胞は，内皮細胞および壁細胞として新生血管へ寄与した。次に，成体への移植に適切な細胞の分化段階を検討するため，分化段階の異なる血管細胞，すなわち，ソート直後のVEGFR2陽性血管前駆細胞と，VEGFR2陽性細胞をさらに3日間培養して初期内皮細胞に分化した細胞（VE-カドヘリン陽性）の移植を比較した。VEGFR2陽性細胞を移植した群では，血管内皮細胞として寄与しているものの他に，内皮以外の細胞として組織内に存在するものが多数（約60％）認められた。一方，初期内皮を移植した群では，ほとんどすべての細胞（95％以上）が内皮細胞として血管に寄与していた。また，VEGFR2陽性細胞移植群では，細胞移植した腫瘍における血流増加は認められなかったが，分化させた血管細胞を移植した群では，有意な血流増加が認

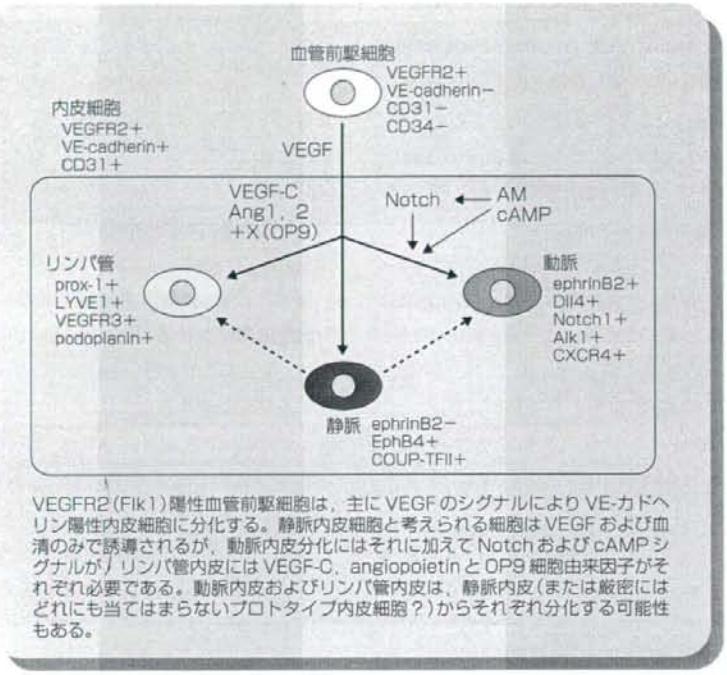

VEGFR2(Flk1)陽性血管前駆細胞は，主にVEGFのシグナルによりVE-カドヘリン陽性内皮細胞に分化する。静脈内皮細胞と考えられる細胞はVEGFおよび血清のみで誘導されるが，動脈内皮分化にはそれに加えてNotchおよびcAMPシグナルが，リンパ管内皮にはVEGF-C，angiopoietinとOP9細胞由来因子がそれぞれ必要である。動脈内皮およびリンパ管内皮は，静脈内皮(または厳密にはどれにも当てはまらないプロトタイプ内皮細胞？)からそれぞれ分化する可能性もある。

図1　VEGFR2陽性細胞からの動静脈リンパ管内皮分化

められた。これらの結果より，成体における血管新生をターゲットとした細胞移植においては，血管前駆細胞のレベルの細胞よりも，やや血管に分化した初期内皮細胞のステージがより有効かつ特異的であると考えられた。このように，ES細胞由来細胞の移植においては，むやみに未分化細胞を移植すればよいわけではなく，ドナー細胞の分化段階とレシピエント側の状況を合わせた至適な分化段階の細胞—おそらくは標的細胞への分化が運命づけられた直近の前駆細胞—を選択する必要があると考えられた。また同時に，移植をされる側においても標的細胞の分化を効率的に促進できる微小環境ができるだけ再現されていることが，有効な再生の実現には重要であると考えられる。

血管再生治療においては，倫理面・安全面・技術面でハードルが低い骨髄細胞や末梢血，G-CSFなどの薬剤を用いた血管新生治療が先行して行われ，優れた効果をあげている。心筋や神経と異なり，既存の組織からの新生が可能な血管においては，細胞による純粋な再生は必ずしも必要ではなく，ES細胞治療がこれらの治療を凌駕して有用であるという知見は今のところない。しかし将来にわたっては，直接的な細胞移植治療のみならずさまざまな血管再生治療のターゲットとなる新たなシーズを生み出し，血管特異的血管新生なども含めさらに治療法を精緻に改善向上させていく上で，ES細胞の血管再生研究における意義は大きいと考えられる。

ヒトES細胞からの血管分化再生

ヒトES細胞を用いた血管細胞分化としては，胚様体を用いてCD31やVE-カドヘリン陽性内皮細胞の誘導と，フローサイトメトリーを用いての純化・再培養，培養下および免疫不全マウスに移植したゲル内における血管構造の形成が報告されている。京都大学のグループは，マウスES細胞と同様にサルES細胞においてもVEGFR2陽性細胞からの内皮細胞・壁細胞の分化[7]，培養下における血管構造形成に成功している。さらに同グループは，2002年より日本最初のヒトES細胞分化研究を輸入ヒトES細胞を用いて開始し，ヒトES細胞においても血管構成細胞の分化誘導と*in vitro*における管腔構造形成，さらにはマウス血管新生モデルにおける新生血管への移植細胞の寄与と血流改善効果を認めることを明らかにした(**図2**)[8,9]。また細胞移植の際に，純化した誘導内皮細胞のみを移植するよりも同時に誘導される壁細胞と混在した形で移植するほうが血管再生効果が高いことを見い出している。同様の現象はES細胞由来心筋細胞移植の動物実験においても，純化